3842 *Organometallics* **2009,** *28,* 3842–3855
DOI: 10.1021/om900176v

ORGANOMETALLICS
Article

A Combined Experimental and Computational Study of Unexpected C−F Bond Activation Intermediates and Selectivity in the Reaction of Pentafluorobenzene with a $(PEt_3)_2Ni$ Synthon

Samuel A. Johnson,* Erin T. Taylor, and Sean J. Cruise

Department of Chemistry & Biochemistry, University of Windsor, Windsor, Ontario, Canada, N9B 3P4

Received March 5, 2009

The reaction of the anthracene adduct $(PEt_3)_2Ni(\eta^2\text{-}C_{14}H_{10})$ with C_6F_5H or C_6F_6 provides a facile route to the isolable dinuclear adducts $[(PEt_3)_2Ni]_2(\mu\text{-}\eta^2\text{:}\eta^2\text{-}C_6F_5H)$ and $[(PEt_3)_2Ni]_2(\mu\text{-}\eta^2\text{:}\eta^2\text{-}C_6F_6)$. The $Ni(PEt_3)_2$ moieties reside on opposite faces of the fluoroarene ring, and bond lengths indicate considerable loss of aromaticity. Solutions of $[(PEt_3)_2Ni]_2(\mu\text{-}\eta^2\text{:}\eta^2\text{-}C_6F_5H)$ with added C_6F_5H convert with >97% selectivity to the *ortho*-F activated compound *trans*-$(PEt_3)_2NiF(2,3,4,5\text{-}C_6F_4H)$. The addition of C_6F_5H to solutions of $[(PEt_3)_2Ni]_2(\mu\text{-}\eta^2\text{:}\eta^2\text{-}C_6F_5H)$ also provided equilibrium amounts of the mononuclear complex $(PEt_3)_2Ni(\eta^2\text{-}C_6F_5H)$ and the C−H activation product *trans*-$(PEt_3)_2NiH(C_6F_5)$ as intermediates. Increased C_6F_5H concentrations accelerate the rate of C−F bond activation. The reaction of $(PEt_3)_4Ni$ with C_6F_5H under similar conditions also provided spectroscopic evidence for the presence of the binuclear adduct $[(PEt_3)_2Ni]_2(\mu\text{-}\eta^2\text{:}\eta^2\text{-}C_6F_5H)$, the mononuclear adduct $(PEt_3)_2Ni(\eta^2\text{-}C_6F_5H)$, and the C−H activation product *trans*-$(PEt_3)_2NiH(C_6F_5)$ in the reaction mixture; however, unlike the C−F bond activation observed from pure $[(PEt_3)_2Ni]_2(\mu\text{-}\eta^2\text{:}\eta^2\text{-}C_6F_5H)$ and C_6F_5H, the reaction of $Ni(PEt_3)_4$ and C_6F_5H yields a mixture of C−F activation products that included the *para*-F and *meta*-F activation products as major products. This indicates that alternate mechanisms of C−F activation dominate with this source of the Ni $(PEt_3)_2$ moiety under these conditions, suggestive of a radical mechanism. Density functional theory calculations were carried out to provide insight into the ^{19}F NMR spectra of these complexes, as well as to gain understanding of the importance of phosphine donor choice in the thermodynamics of the interconversion of the dinuclear complexes, mononuclear complexes, and C−H activation products.

Introduction

Many modern pharmaceuticals and agrochemicals contain partially fluorinated substituents,[1,2] which are commonly accessed using selective fluorinating reagents.[3] The use of transition metal complexes in the catalytic activation[4] and functionalization of C−F or C−H bonds in partially fluorinated organics has been envisioned as an attractive alternate synthetic route to these species,[5,6] with the potential to prepare compounds with previously unobtainable patterns of fluorination.

Zero-valent nickel phosphine complexes are attractive for these transformations, not only due to the relatively low cost of nickel compared to the heavier platinum group metals and the commercial availability of the phosphine donor ligands, but also because DFT calculations have predicted that these nickel complexes should exhibit a decreased thermodynamic propensity for C−H bond activation compared to their heavier analogues,[7] and thus might be expected to undergo selective C−F bond activation even in the presence of more reactive C−H bonds.[8−10] Although there are a plethora of examples of the selective C−F bond activation of perfluorinated arenes,[11] only a few examples of the selective activation

*To whom correspondence should be addressed. E-mail: sjohnson@uwindsor.ca. Fax: (519) 973-7098.

(1) Mueller, K.; Faeh, C.; Diederich, F. *Science* **2007**, *317*, 1881–1886.
(2) Brooke, G. M. *J. Fluorine Chem.* **1997**, *86*, 1–76.
(3) (a) Begue, J.-P.; Bonnet-Delpon, D. *J. Fluorine Chem.* **2006**, *127*, 992–1012. (b) Prakash, G. K. S.; Chacko, S. *Curr. Opin. Drug Discovery Dev.* **2008**, *11*, 793–802. (c) Shimizu, M.; Hiyama, T. *Angew. Chem., Int. Ed.* **2005**, *44*, 214–231.
(4) (a) Schaub, T.; Backes, M.; Radius, U. *J. Am. Chem. Soc.* **2006**, *128*, 15964–15965. (b) Bohm, V. P. W.; Gstottmayr, C. W. K.; Weskamp, T.; Herrmann, W. A. *Angew. Chem., Int. Ed.* **2001**, *40*, 3387–3389. (c) Young, R. J.Jr; Grushin, V. V. *Organometallics* **1999**, *18*, 294–296.
(5) (a) Kiplinger, J. L.; Richmond, T. G.; Osterberg, C. E. *Chem. Rev.* **1994**, *94*, 373–431. (b) Burdeniuc, J.; Jedlicka, B.; Crabtree, R. H. *Chem. Ber.* **1997**, *130*, 145–154. (c) Braun, T.; Perutz, R. N. *Chem. Commun.* **2002**, 2749–2757. (d) Braun, T.; Perutz, R. N. *Spec. Publ.−R. Soc. Chem.* **2003**, *287*, 136–151. (e) Mazurek, U.; Schwarz, H. *Chem. Commun.* **2003**, 1321–1326. (f) Richmond, T. G. *Angew. Chem., Int. Ed.* **2000**, *39*, 3241–3244.
(6) Perutz, R. N. In *Comprehensive Organometallic Chemsitry III*; Crabtree, R. H., Mingos, M. P., Eds.; Elsevier: New York, 2007, ; Vol. *1*, pp 725−756.
(7) Reinhold, M.; McGrady, J. E.; Perutz, R. N. *J. Am. Chem. Soc.* **2004**, *126*, 5268–5276.
(8) (a) Clot, E.; Oelckers, B.; Klahn, A. H.; Eisenstein, O.; Perutz, R. N. *Dalton Trans.* **2003**, 4065–4074. (b) Clot, E.; Besora, M.; Maseras, F.; Megret, C.; Eisenstein, O.; Oelckers, B.; Perutz Robin, N. *Chem. Commun.* **2003**, 490–491.
(9) Liu, W.; Welch, K.; Trindle, C. O.; Sabat, M.; Myers, W. H.; Harman, W. D. *Organometallics* **2007**, *26*, 2589–2597.
(10) Johnson, S. A.; Huff, C. W.; Mustafa, F.; Saliba, M. *J. Am. Chem. Soc.* **2008**, *130*, 17278–17280.
(11) (a) Schaub, T.; Radius, U. *Chem−Eur. J.* **2005**, *11*, 5024–5030. (b) Torrens, H. *Coord. Chem. Rev.* **2005**, *249*, 1957–1985.

 Published on Web 05/19/2009

of the more synthetically useful partially fluorinated arenes have been reported.[12,13] For example, the oxidative addition of C_6F_6 to a Ni(0) phosphine complex, obtained from the reaction of PEt_3 with $Ni(COD)_2$, was reported as early as 1977,[14] albeit with difluorophosphoranes (F_2PR_3) as unwanted byproducts when excess fluoroarene is used.[15] However, the reaction of C_6F_5H with $Ni(PEt_3)_4$ was reported to be unselective and produced a mixture of all three possible C−F activation products, along with phosphoranes and 1,2,4,5-tetrafluorobenzene.[15]

The observation of difluorophosphoranes in the reaction of $Ni(PEt_3)_4$ with C_6F_6 suggests that excess phosphine may interfere with the reaction in these systems. The presence of excess phosphine may also decrease the equilibrium concentration of the species $Ni(PEt_3)_2$ and $Ni(PEt_3)_3$ in favor of the 18-electron complex $Ni(PEt_3)_4$. This may explain the lack of selectivity in the reaction of pentafluorobenzene with $Ni(PEt_3)_4$; this coordinatively saturated species is probably only suited to oxidative addition reactions by a mechanism that involves electron transfer.[16] Herein we use the anthracene adduct $(PEt_3)_2Ni(\eta^2\text{-}C_{14}H_{10})$,[17] which provides an opportunity to examine the reaction of fluorinated arenes with a source of the $(PEt_3)_2Ni$ moiety in the absence of excess phosphine.

Results and Discussion

Synthesis and Characterization of a Dinuclear $Ni(PEt_3)_2$ Adduct of C_6F_5H. The reaction of a red solution of the $(PEt_3)_2Ni$-anthracene adduct $(PEt_3)_2Ni(\eta^2\text{-}C_{14}H_{10})$[17] with ~4 equiv of pentafluorobenzene in pentane results in an immediate precipitation of anthracene from the solution and a color change to yellow. Analysis of the crude solution by NMR spectroscopy reveals the adduct $[(PEt_3)_2Ni]_2(\mu\text{-}\eta^2\text{:}\eta^2\text{-}C_6F_5H)$ (**1**) as the only fluoroaromatic-containing product, as shown in eq 1. Complex **1** was readily isolated by filtering off the anthracene produced, followed by crystallization from the pentane solution at −40 °C. A moderate excess of C_6F_5H is required to drive this reaction to completion, indicative of rapid equilibrium. This was verified by the addition of anthracene to the isolated complex, which results in a slight back reaction to produce the red $(PEt_3)_2Ni$-anthracene adduct and free C_6F_5H, as verified by ^1H, ^{19}F, and $^{31}P\{^1H\}$ NMR spectroscopy.

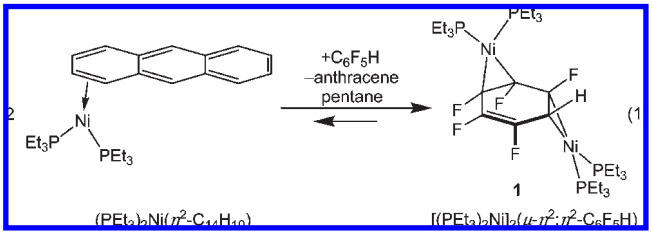

Single crystals suitable for structural analysis by X-ray crystallography were obtained from this synthesis, and an ORTEP depiction of the solid-state molecular structure is shown in Figure 1. X-ray crystallographic collection and refinement parameters are included in Table 1. The structure of **1** features two molecules in the asymmetric unit that have identical connectivities. A pair of $(PEt_3)_2Ni$ fragments are bound to opposite faces of the C_6F_5H ring. The structure features a disorder of the aromatic hydrogen atom. This was modeled as a 2-fold disorder, with a 50% occupancy of the hydrogen atom on both C(1) and C(4), although it is impossible to rule out smaller partial occupancies at other sites.

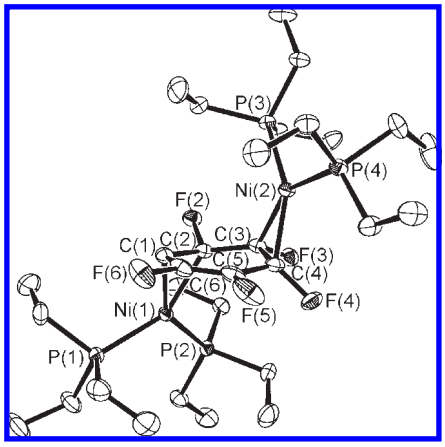

Figure 1. ORTEP depiction of the solid-state molecular structure of **1** as determined by X-ray crystallography. Hydrogen atoms are omitted for clarity, and the 2-fold disorder of the hydrogen atom associated with the aromatic ring is not shown. The 30% probability ellipsoids are shown. Selected bond lengths (Å): Ni(1)−C(1), 1.935(3); Ni(1)−C(2), 1.957(3); Ni(1)−P(2), 2.1732(9); Ni(1)−P(1), 2.1790(9); Ni(2)−C(4), 1.933(3); Ni(2)−C(3), 1.952(3); Ni(2)−P(3), 2.1765(9); Ni(2)−P(4), 2.1803(9); C(1)−C(2), 1.437(4); C(1)−C(6), 1.444(5); C(2)−C(3), 1.460(4); C(3)−C(4), 1.431(4); C(4)−C(5), 1.447(5); C(5)−C(6), 1.322(5); F(1)−C(1), 1.310(5); F(2)−C(2), 1.408(3); F(3)−C(3), 1.411(3); F(4)−C(4), 1.335(4); F(5)−C(5), 1.365(4); F(6)−C(6), 1.360(4).

Table 1. Crystallographic Data for Compounds 1, 2, and 5

	1	**2**	**5**
empirical formula	$C_{30}H_{61}F_5Ni_2P_4$	$C_{18}H_{31}F_5NiP_2$	$C_{30}H_{60}F_6Ni_2P_4$
fw	757.56	463.08	775.56
cryst syst	monoclinic	orthorhombic	monoclinic
a (Å)	19.195(3)	9.224(3)	19.3710(19)
b (Å)	10.0767(16)	9.411(3)	10.0468(10)
c (Å)	41.554(6)	25.879(8)	41.310(4)
α (deg)	90.	90.	90.
β (deg)	105.297(6)	90.	105.496(4)
γ (deg)	90.	90.	90.
V (Å^3)	7753(2)	2246.4(12)	7747.4(13)
space group	*P*2/*c*	*P*2(1)2(1)2(1)	*P*2/*c*
Z value	8	4	8
D_{calc} (g/cm^3)	1.298	1.369	1.33
μ(Mo Kα) (mm^{-1})	1.178	1.046	1.185
temperature (K)	173(2)	173(2)	173(2)
$2\theta_{max}$ (deg)	55.0	50.0	55.0
total no. of reflns	83 977	21 391	84 942
no. unique reflns; R_{int}	17 559; 0.033	3950; 0.046	17 524; 0.037
transmn factors	0.81−0.66	0.90−0.73	0.94−0.79
no. with $I \geq 2\sigma(I)$	14 997	3763	13 992
no. variables	781	241	781
reflns/params	19.2	15.6	17.9
R; wR_2 (all data)	0.060; 0.12	0.053; 0.14	0.053; 0.098
GOF	1.147	1.108	0.976
residual density (e$^-$/Å^3)	1.135; −0.555	1.032; −0.350	0.882; −0.839

(12) (a) Whittlesey, M. K.; Perutz, R. N.; Moore, M. H. *Chem. Commun.* **1996**, 787–788. (b) Edelbach, B. L.; Jones, W. D. *J. Am. Chem. Soc.* **1997**, *119*, 7734–7742.
(13) Schaub, T.; Fischer, P.; Steffen, A.; Braun, T.; Radius, U.; Mix, A. *J. Am. Chem. Soc.* **2008**, *130*, 9304–9317.
(14) Fahey, D. R.; Mahan, J. E. *J. Am. Chem. Soc.* **1977**, *99*, 2501–2508.
(15) Cronin, L.; Higgitt, C. L.; Karch, R.; Perutz, R. N. *Organometallics* **1997**, *16*, 4920–4928.
(16) Tsou, T. T.; Kochi, J. K. *J. Am. Chem. Soc.* **1979**, *101*, 6319–6332.
(17) Stanger, A.; Boese, R. *J. Organomet. Chem.* **1992**, *430*, 235–243.

The structure of **1** features significant differences in the Ni−C distances; the Ni(1)−C(1) and Ni(2)−C(4) bond lengths of 1.935(3) and 1.933(3) Å, respectively, are slightly shorter than the Ni(1)−C(2) and Ni(2)−C(3) bond lengths, which are 1.957(3) and 1.952(3) Å, respectively. The back-bonding of the $Ni(PEt_3)_2$ moieties to the arene ring results in significant elongation of the coordinated double bonds from typical aromatic values, with C(1)−C(2) and C(3)−C(4) distances of 1.437(4) and 1.431(4) Å, respectively, as well as considerable nonplanarity of the F-substituents. The remaining C−C bond lengths of the C_6F_5H moiety are also significantly perturbed by the back-donation. The C(5)−C(6) distance of 1.322(5) Å is close to that expected for a double bond, whereas the C(2)−C(3), C(4)−C(5), and C(6)−C(1) distances of 1.460(4), 1.447(5), and 1.444(5) Å, respectively, are closer to the values expected for single bonds.

There appears to be little precedent for such dinuclear complexes bearing two metal centers η^2-coordinated to a single aromatic ring[18] in the C−F activation literature, despite related examples relevant to C−H activation.[19] Alternate structures were suggested for related dinuclear nickel complexes of hexakis(trifluoromethyl)benzene, but were based solely on NMR data in the absence of X-ray structural data, and it seems likely that the structures of these complexes may be analogous to **1**.[20] The bonding in **1** is similar to that previously observed in the complex $[(^tBu_2PCH_2CH_2P^tBu_2)_2Ni]_2(\mu\text{-}\eta^2\text{:}\eta^2\text{-}C_6H_6)$; however, it is notable that the reaction of this complex with C_6F_6 did not generate the dinuclear analogue $[(^tBu_2PCH_2CH_2P^tBu_2)_2Ni]_2(\mu\text{-}\eta^2\text{:}\eta^2\text{-}C_6F_6)$, but rather the mononuclear adduct $(^tBu_2PCH_2CH_2P^tBu_2)_2Ni(\eta^2\text{-}C_6F_6)$.[21]

The room-temperature 300 MHz ^1H NMR spectrum of **1** in C_6D_6 features an upfield-shifted broad multiplet for the hydrogen bound to the aromatic moiety at δ 3.12 and resonances at δ 1.01 and 1.61 for the PEt_3 ligands. The 1:36:24 integration of these peaks is consistent with the formulation $[(PEt_3)_2Ni]_2(\mu\text{-}\eta^2\text{:}\eta^2\text{-}C_6F_5H)$ assigned from X-ray crystallography. The 282 MHz $^{19}F\{^1H\}$ NMR spectrum at room temperature displays five broad featureless peaks at δ −134.9, −144.0, −155.2, −158.7, and −185.4 with line widths varying from 107 to 153 Hz. The broadness of these peaks is indicative of a fluxional process, but the presence of five, rather than three, fluorine environments indicates that rapid exchange via repeated concerted 1,2-shifts of both $Ni(PEt_3)_2$ groups is not occurring at room temperature. A variable-temperature ^{19}F NMR study was performed to gain further insight into the nature of this fluxional process, and the experimental spectra are shown at the top of Figure 2. Upon cooling below room temperature, four of the resonances exhibit temperature-dependent chemical shifts, but of these four, only the peaks at −144.0, −155.2, and −185.4 broaden significantly. Further cooling to 200 K does not lead to any observed decoalescence, but rather the sharpening of these resonances into unresolved multiplets.

The observation of line broadening without any apparent decoalescence is atypical for fluxional processes and

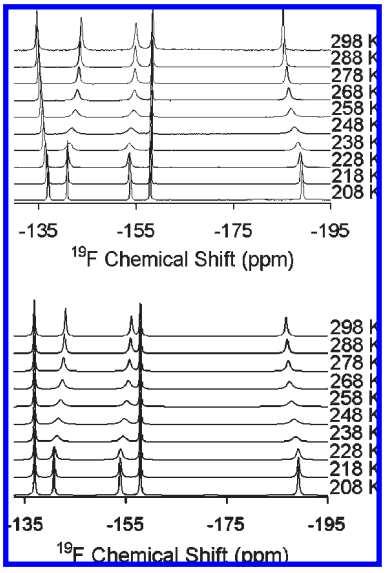

Figure 2. Experimental (top) and modeled (bottom) variable-temperature ^{19}F NMR spectra for compound **1** obtained at 282 MHz.

Scheme 1

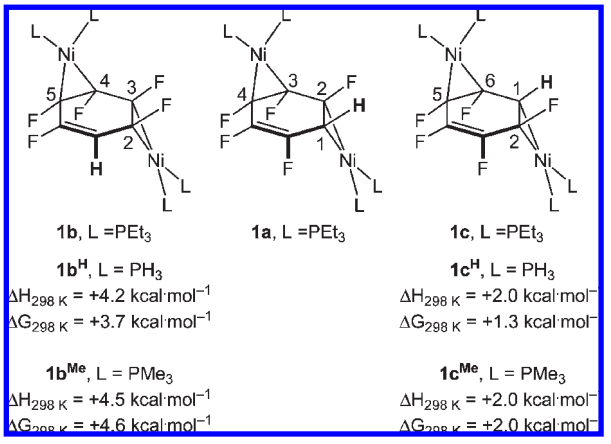

provides insight into the nature of the chemical exchange in this compound. It was hypothesized that the energy difference between the three possible isomers of $[(PEt_3)_2Ni]_2(\mu\text{-}\eta^2\text{:}\eta^2\text{-}C_6F_5H)$ might strongly favor one isomer, but allow for the conversion to an equilibrium amount of a second low-energy isomer at higher temperatures. Density functional theory (DFT) calculations using the B3LYP functional and TZVP basis set were performed on the model complexes $[(PH_3)_2Ni]_2(\mu\text{-}\eta^2\text{:}\eta^2\text{-}C_6F_5H)$ **1a**−**c**$^{\mathbf{H}}$ and $[(PMe_3)_2Ni]_2(\mu\text{-}\eta^2\text{:}\eta^2\text{-}C_6F_5H)$ **1a**−**c**$^{\mathbf{Me}}$, to estimate the energy differences between the three isomers of the model complexes, shown in Scheme 1. Calculations with both PH_3 and PMe_3 as the model phosphines agree with the crystallographic observation that the lowest energy isomer is **1a**, which has the nickel centers at the 1,2- and 3,4-positions of the pentafluorophenyl ring, where the aromatic carbon bearing the hydrogen substituent is considered the 1-position. Conversion to the isomers with the nickel centers at the 2,3- and 4,5-positions, which are labeled **1b**$^{\mathbf{H}}$ and **1b**$^{\mathbf{Me}}$ for the PH_3- and PMe_3-containing model complexes, is predicted to have a $\Delta G_{298\ K}$ of 3.7 and 4.6 kcal·mol^{-1}, respectively. The isomer with the nickel centers at the 1,2- and 5,6-positions, labeled **1c**, is predicted to be slightly more favorable than **1b**, but still

(18) Beck, V.; O'Hare, D. *J. Organomet. Chem.* **2004**, *689*, 3920–3938.
(19) Chin, R. M.; Dong, L.; Duckett, S. B.; Jones, W. D. *Organometallics* **1992**, *11*, 871–876.
(20) (a) Stone, F. G. A.; Browning, J.; Cundy, C. S.; Green, M. *J. Chem. Soc. A* **1971**, 448–452. (b) Browning, J.; Green, M.; Spencer, J. L.; Stone, F. G. A. *J. Chem. Soc., Dalton Trans.* **1974**, 97–101.
(21) Bach, I.; Poerschke, K.-R.; Goddard, R.; Kopiske, C.; Krueger, C.; Rufinska, A.; Seevogel, K. *Organometallics* **1996**, *15*, 4959–4966.

higher energy than **1a**. The conversion of $\mathbf{1a^H}$ to $\mathbf{1c^H}$ is predicted to have a $\Delta G_{298\ K}$ of 1.3 kcal·mol^{-1}, and the conversion of $\mathbf{1a^{Me}}$ to $\mathbf{1c^{Me}}$ is predicted to have a $\Delta G_{298\ K}$ of 2.0 kcal·mol^{-1}. The differences in Gibbs free energies for the PMe_3 model complexes can be used to estimate the equilibria between the analogous isomers bearing PEt_3. At 298 K, it is anticipated that ~97% of the sample will exist as isomer 1a, the remaining 3% as **1c**. The 4.6 kcal·mol^{-1} free energy difference for **1b** indicates that it will be a negligible 0.04% of the sample at 298 K. At 200 K, the ratios change considerably, and the predicted percentages of **1a** and **1c** are 99.4 and 0.6, respectively.

To create a model to fit the observed variable-temperature ^{19}F NMR spectra, chemical shifts for the **1c** isomer are required, but were not available experimentally; however, it was found that DFT could provide an accurate estimate of the ^{19}F NMR chemical shifts for this class of complexes. The calculated chemical shifts for the model complexes $[(PMe_3)_2Ni]_2(\mu\text{-}\eta^2\text{:}\eta^2\text{-}C_6F_5H)$, $\mathbf{1a^{Me}}$, are δ −136.5, −146.3, −154.6, −163.3, and −182.0, which has a maximum error of 4.6 ppm and a root-mean-square error of 3.1 ppm compared to the experimentally observed spectrum for **1**. This accuracy in predicted shifts described further confirms that **1a** is the predominant isomer in solution. It also allows assignment of the experimentally observed resonances at δ −134.9, −144.0, −155.2, −158.7, and −185.4 as the 2, 6, 3, 5, and 4 sites of the C_6F_5H moiety, respectively. The addition of C_6F_5D to **1** (vide infra) generated an equilibrium amount of $[(PEt_3)_2Ni]_2(\mu\text{-}\eta^2\text{:}\eta^2\text{-}C_6F_5D)$, **1-*d*$_1$**, which allowed experimental verification that the peaks at δ −134.9 and −144.0 in **1** are *ortho* to the C−H/D bond, due to the observable 0.3 ppm isotope shift[22] of these resonances compared to **1-*d*$_1$**. In comparison, the alternate isomer **1b** is predicted to exhibit ^{19}F NMR resonances at δ −149.3, −159.3, −160.8, −169.6, and −189.6 for the 6, 4, 3, 2, and 5 sites of the aromatic ring. The **2c** isomer has predicted ^{19}F NMR resonances at δ −134.2, −156.8, −159.4, −178.7, and −187.6 for the 6, 4, 3, 2, and 5 sites of the aromatic ring. That **1b** and **1c** are not the predominant isomers in solution for **1** is confirmed by the large difference between the observed and predicted shifts; the maximum errors in predicted shifts are 15.3 and 20 ppm, and the root-mean-square errors are 10.0 and 11.1 ppm, respectively.

Two plausible intramolecular mechanisms can be envisioned for the exchange process observed in the ^{19}F NMR of **1a**. One possibility is that both metals do a simultaneous 1,2-shift in the same direction around the ring, which is shown at the top of Scheme 2. The simultaneous clockwise or counterclockwise 1,2-shifts starting from **1a** can produce either isomer **1b** or **1c**, but further shifts are not consistent with the observed variable-temperature ^{19}F spectra, because this would allow for the exchange of the pairs of *ortho*- and *meta*-fluorine environments and result in only three fluorine environments in the high-temperature spectra. The requirement that only certain 1,2-shifts can occur is counterintuitive, particularly because an additional counterclockwise 1,2-shift of both Ni fragments in **1c** would generate the lowest energy isomer **1a**.

This limitation is not encountered with an alternate mechanism of exchange between the three isomers that involves 1,3-shifts of only one Ni moiety at a time, which could occur via an η^4-bound intermediate.[17] This mechanism of exchange is shown at the bottom of Scheme 2. The localized formal double and single bonds of the fluorinated rings are maintained despite the 1,3-shifts. Thus even repeated 1,3-shifts to generate both the **1b** and **1c** isomers do not exchange the 2,6-*ortho* and 3,5-*meta* fluorine environments.

These two mechanisms exchange different ^{19}F environments and thus should be differentiable using the energies and ^{19}F NMR chemical shifts determined by DFT calculations. The simultaneous 1,2-shifts convert the F_2, F_3, F_4, F_5, and F_6 positions of the major isomer **1a** to the F_6, F_5, F_4, F_3, and F_2 positions of the predicted minor isomer **1c**, whereas the consecutive 1,3-shifts convert the F_2−F_6 positions of the major isomer **1a** to the identically numbered F_2−F_6 positions of the **1c** isomer. Table 2 summarizes the calculated ^{19}F NMR chemical shifts for **1a**, the chemical shifts they exchange with in **1c** via either mechanism, and the differences in shifts.

Only the mechanism that involves 1,3-shifts of the Ni-$(PEt_3)_2$ moieties in **1a** is consistent with the observed variable-temperature ^{19}F NMR spectra, because it predicts that an exchange with the thermally accessible **1c** isomer should lead to the most broadening and shifting of the resonances

Table 2. Experimental 1a and Calculated $\mathbf{1c^{Me}}$ NMR Shifts in ppm versus $CFCl_3$[a]

label **1a** ^{19}F in **1a** shifts	$\mathbf{1c^{Me}}$ ^{19}F chemical shifts via 1,2-shift	change in ^{19}F chemical shifts via 1,2-shift	$\mathbf{1c^{Me}}$ ^{19}F chemical shifts via 1,3-shift	change in ^{19}F chemical shifts via 1,3-shifts
F_2 −136.4	−178.7	**42.3**	−134.2	−2.2
F_6 −146.3	−134.2	**−12.1**	−178.7	**32.4**
F_3 −154.6	−159.4	4.8	−187.7	**33.1**
F_5 −163.3	−187.7	**24.4**	−159.4	−3.9
F_4 −182.0	−156.8	**−25.2**	−156.8	**−25.2**

[a] Bolded changes in chemical shift indicate resonances that are predicted to be most shifted compared to **1a** by the proposed exchange mechanism.

Scheme 2

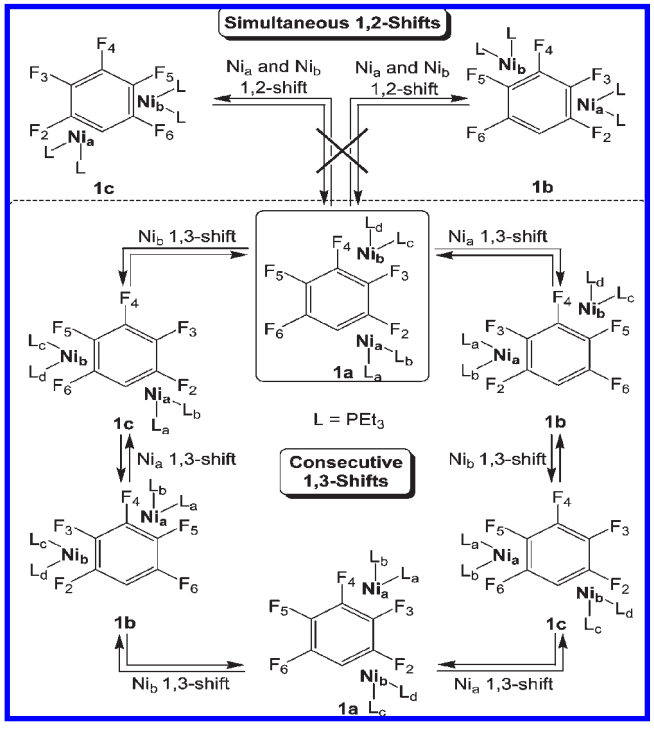

(22) Keen, A. L.; Doster, M.; Johnson, S. A. *J. Am. Chem. Soc.* **2007**, *129*, 810–819.

associated with the F_6 (δ −146.3), F_3 (δ −154.6), and F_4 (δ −182.0) nuclei of **1a**, as labeled in Scheme 2, due to the large chemical shift differences of 32.4, 33.1, and −25.2 ppm between these two isomers. The model not only correctly predicts which resonances should broaden at higher temperatures but also correctly predicts the direction in which the chemical shifts should change. The F_2 and F_5 nuclei have negligibly different shifts in the two isomers if the exchange occurs via 1,3-shifts, which is consistent with the fast-exchange limit being observed even at low temperatures.

A quantitative model of the variable-temperature ^{19}F NMR spectra from 208 to 298 K was performed using the experimentally observed low-temperature chemical shifts for **1** and using the calculated shifts of **1c** for the second lowest energy isomer. Attempts to model the spectrum using the DFT-calculated 2 kcal·mol^{-1} energy difference between **1a** and **1c** failed; the best fit to the experimental data was obtained by using a 1.5 kcal·mol^{-1} energy difference. These model spectra are shown at the bottom of Figure 2 and correctly predict the main features of the observed spectrum. The rate constant data from this analysis predicts an Arrhenius activation energy of 10 kcal·mol^{-1}.

At higher temperatures an alternate exchange pathway appears to be accessible, and the pair of *meta* resonances observed at −155.2, −158.7 in the room-temperature spectrum coalesce at 328 K. Similarly, the *ortho* resonance at δ −134.9, −144.0 in the room-temperature spectrum broaden significantly and near coalescence at 338 K. These high-temperature NMR spectra can be modeled using the Arrhenius equation to estimate a 19.5 kcal·mol^{-1} activation energy for this process or the Eyring equation to estimate a $\Delta H^{\ddagger}$ of 18.8 kcal·mol^{-1} and a $\Delta S^{\ddagger}$ of 7.3 kcal·K^{-1}·mol^{-1}.

The room-temperature 121.5 MHz $^{31}P\{^1H\}$NMR spectrum of **1** in C_6D_6 features a broad asymmetric multiplet at δ 18, with a peak width at half height of 870 Hz. A variable-temperature $^{31}P\{^1H\}$ NMR study was performed in C_7D_8 and is shown in Figure 3. At 243 K a slow exchange limit spectrum is obtained, with four distinct muliplets, which is consistent with the solid-state structure. No further change is observed on cooling as low as 223 K. Upon warming, these peaks broaden and coalesce near 293 K. These spectra are readily modeled from 263 to 293 K by assuming only two pairs of ^{31}P environments are in exchange, namely, those at δ 24.7 and 17.5 as well as the pair of shifts at δ 20.6 and 14.0. This simple model predicts that two resonances should be observed at higher temperatures; however, the nature of this exchange is clearly more complicated, with additional exchange pathways available at higher temperatures that exchange all four phosphorus environments. Thus, rather than sharpening at higher temperatures, the signals all coalesce to give a broad resonance at 303 K, which could not be modeled. At higher temperatures, decomposition by rapid C−F bond activation occurred, as evidenced by the appearance of a doublet at δ 12.5. This decomposition prevented the collection of a fast exchange limit spectrum.

The rates of exchange modeled from 263 to 293 K can be used to estimate an Arrhenius activation energy of 13.3 kcal·mol^{-1} or plotted using the Eyring equation to estimate a $\Delta H^{\ddagger}$ of 12.7 kcal·mol^{-1} and a $\Delta S^{\ddagger}$ of −13.2 kcal·K^{-1}·mol^{-1}. These values are significantly larger than the Arrhenius activation energy of 10.0 kcal·mol^{-1} predicted for the conversion of **1a** and **1c** from the variable-temperature ^{19}F NMR spectra, which implies that the conversion between **1a** and **1c** does not exchange any

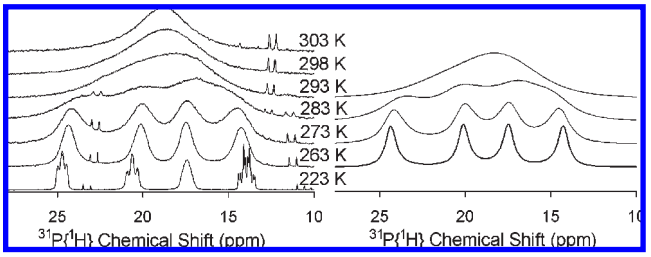

Figure 3. Variable-temperature $^{31}P\{^1H\}$ NMR spectra for complex **1** (left), obtained at 121.5 MHz, and modeled spectra (right).

phosphorus environments. A 243 K ^{31}P-COSY spectrum confirms that the phosphine environments in exchange are on different Ni centers; cross-peaks are observed between the ^{31}P resonances at δ 24.7 and 14.0, as well the resonances at δ 20.6 and 17.5, not the phosphorus environments in exchange form 263 to 293 K. Thus the exchange process observed in the $^{31}P\{^1H\}$ NMR spectra between 263 to 293 K must involve multiple 1,3-shifts that exchange the identities of the Ni_a and Ni_b centers shown in Scheme 2. The only mechanism that is viable for the exchange of pairs of phosphorus environments is shown in Scheme 2. The Ni-$(PEt_3)_2$ fragments must make three consecutive 1,3-shifts to exchange the locations of the Ni_a and Ni_b in the **1a** isomers on the top and the bottom of the scheme. As drawn, these shifts allow for the exchange of the PEt_3 moieties labeled L_a and L_c as well as L_b and L_d. An alternate motion where the $Ni(PEt_3)_2$ moieties spin as they undergo shifts, related examples of which have been observed in mononuclear aromatic adducts of related mononuclear Ni complexes[23] and calculated for mononuclear C_6F_6 adducts,[7] is not viable; the exchange in the clockwise and counterclockwise directions depicted in Scheme 2 would result in the exchange of different pairs of phosphorus nuclei, but microscopic reversibility requires that both pathways have the same barrier. The observation that the barrier of ^{31}P environment exchange is greater than that of the barrier of ^{19}F exchange is consistent with the fact that the ^{31}P exchange requires the intermediacy of the highest energy isomer, **1b**, the activation barrier to which is presumably greater than that between **1a** and **1c**.

Selective *Ortho* C−F bond Activation of C_6F_5H. In the presence of added C_6F_5H, solutions of **1** in a variety of hydrocarbon or ethereal solvents convert to give primarily (>97%) the complex derived from C−F bond activation at the 1-position, *trans*-$(PEt_3)_2NiF(2,3,4,5\text{-}C_6F_4H)$ (**2**), as shown in eq 2. The rate of C−F bond activation is strongly dependent on the conditions (vide infra), but is slower than the formation of **1** shown in eq 1.

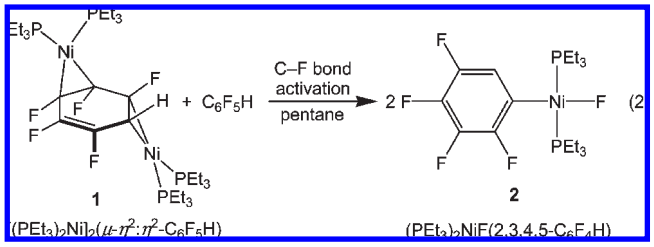

Crystals suitable for analysis by X-ray crystallography were obtained from slow evaporation of a pentane solution,

(23) Atesin, T. A.; Li, T.; Lachaize, S.; Garcia, J. J.; Jones, W. D. *Organometallics* **2008**, *27*, 3811–3817.

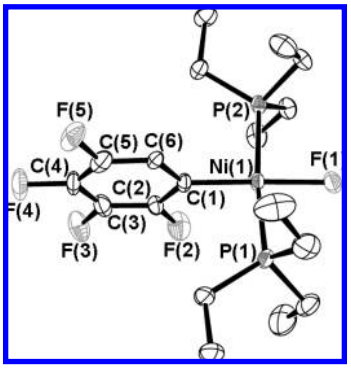

Figure 4. ORTEP depiction of the solid-state molecular structure of **2** as determined by X-ray crystallography. Hydrogen atoms are omitted for clarity, and 30% probability ellipsoids are shown. Selected bond lengths (Å): Ni(1)−C(1), 1.858(4); Ni(1)−F(1), 1.916(3); Ni(1)−P(2), 2.1899(14); Ni(1)−P(1), 2.1907(14). Selected bond angles (deg): P(2)−Ni(1)−P(1), 171.41(6); C(1)−Ni(1)−F(1), 178.0(2); P(1)−Ni(1)−C(1), 92.62(14); P(2)−Ni(1)−C(1), 93.35(14); Ni(1)−C(1)−C(2), 121.67(35); Ni(1)−C(1)−C(6), 121.35(36); C(2)−C(1)−C(6), 117.0(4).

and an ORTEP depiction of the solid-state molecular structure is shown in Figure 4. The connectivity in **2** demonstrates that it is produced from the activation of the fluorine substituent *ortho* to hydrogen in C_6F_5H. The structural features of square-planar **2** resemble those of the known analogue *trans*-$(PEt_3)_2NiF(C_6F_5)$.[15] The Ni−C(1) bond length in **2** of 1.858(4) Å is only 0.022(6) Å longer than that of *trans*-$(PEt_3)_2NiF(C_6F_5)$, whereas the Ni(1)−F(1) distance of 1.916(3) Å is longer by a more significant 0.080(6) Å. The most notable difference in angles is the C(2)−C(1)−C(6) angle of 117.0(4)°, which is significantly larger than the previously reported analogous angle in *trans*-$(PEt_3)_2NiF(C_6F_5)$ of 112.4(7)°.[15]

The connectivity of **2** was confirmed using ^{19}F NMR spectroscopy, where four aromatic F multiplets are observed at δ −116.9, −142.7, −160.2, and −166.1 and the Ni fluoride resonance at δ −380.7 is a doublet of triplets with a $^4J_{FF}$ of 11.0 Hz to a single *ortho*-F and a 47.6 Hz coupling to two identical phosphorus nuclei. The $^{31}P\{^1H\}$ NMR spectrum consists of a doublet of multiplets centered at δ −12.5, with a 47.6 Hz coupling to the terminal fluoride and unresolved coupling to the remaining aromatic fluorine nuclei. The ^1H NMR features a complex multiplet at δ 6.89, corresponding to the aromatic hydrogen.

Equilibrium Mononuclear Adduct Formation and C−H Bond Activation. The selectivity of the $Ni(PEt_3)_2$ moiety for C−F bond activation at the *ortho*-F is atypical for pentafluorobenzene C−F activation. Nucleophilic substitution at C_6F_5H typically occurs at the 3-position, *para* with respect to the hydrogen substituent, and in some cases in the 2-position, *meta* with respect to the H substituent. Nucleophilic substitution at the 1-position is only rarely observed, and never with high selectivity.[2,24] Unselective *ortho* activation products are known,[15,25] but of the few previous examples of transition metal complexes capable of selective C−F bond activation in pentafluorobenzene, all occur in the *para*-position.[12,13,26] A recent example of catalytic hydrodefluorination of pentafluorobenzene to produce 1,2,4,5-tetrafluorobenzene has been reported, but is proposed to occur via aryne formation from a pentafluorophenyl complex formed by C−H bond activation.[27] Regardless of the differing mechanism, this suggests that an initial interaction of the C−H bond with the $Ni(PEt_3)_2$ fragment could conceivably be responsible for the unexpected *ortho* C−F bond selectivity in the formation of **2**, and thus attempts were made to gain insight into the mechanism of this reaction.

The mechanism of C−F bond oxidative addition in fluorinated aromatics commonly occurs via an intermediate where the arene complex is η^2-coordinated to the metal complex,[28] although alternate mechanisms that bypass this intermediate[9] or involve nucleophilic attack or electron transfer are well-documented.[6,12] The hexafluorobenzene and octafluoronaphthalene adducts $(^tBu_2PCH_2CH_2P^tBu_2)_2Ni(\eta^2\text{-}C_6F_6)$[21] and $(PEt_3)_2Ni(\eta^2\text{-}C_{10}F_8)$[29] are known, and both undergo subsequent slow C−F bond activation, which supports the presence of arene-coordinated intermediates in the reaction of Ni(0) phosphine adducts with fluorinated aromatics. However, recent evidence suggests that even this traditional mechanism may feature surprising subtleties, such as phosphine assistance[30] in the C−F bond cleavage step and rapid, reversible C−H bond activation prior to C−F bond activation.[10]

A mechanism that involves a mononuclear intermediate is still feasible for the conversion of **1** to **2**, if the mononuclear species **3** is generated in equilibrium with **1** and C_6F_5H prior to the C−F activation step, as shown in Scheme 3 as mechanism A. We previously observed that the reaction of the phenanthrene adduct $(PEt_3)_2Ni(\eta^2\text{-}C_{10}H_{14})$ with 1,2,4,5-tetrafluorobenzene produces an equilibrium amount of the C−H activation product *trans*-$(PEt_3)_2NiH(2,3,5,6\text{-}C_6F_4H)$.[10] Thus it seems likely that if the mononuclear adduct **3** is an intermediate, hydride **4** could also be present in equilibrium, as shown in Scheme 3, mechanism A. Either **3** or **4** could conceivably convert to **2**.

An alternate pathway, labeled mechanism B in Scheme 3, where initial C−F bond activation occurs directly from the binuclear adduct **1**, is also plausible. This intermediate could then react with C_6F_5H to generate the C−F activation product **2** and half an equivalent of **1**. This latter mechanism could explain the unusual selectivity of C−F bond activation. More complicated mechanisms that involve radical intermediates that arise from electron transfer cannot be excluded, but are omitted here due to lack of supporting evidence.

The addition of C_6F_5H (0.5−90 equiv) to a solution of **1** in C_6D_6 produced solutions that still contain **1**, as determined by ^1H, ^{19}F, and $^{31}P\{^1H\}$ NMR spectroscopy; however, two other species were also observed in equilibrium amounts. The highest concentration equilibrium species is assignable

(24) (a) Burdon, J. *Tetrahedron* **1965**, *21*, 3373–3380. (b) Brooke, G. M.; Burdon, J.; Tatlow, J. C. *J. Chem. Soc.* **1962**, 3253–3255. (c) Castle, M. D.; Plevey, R. G. *J. Fluorine Chem.* **1973**, *2*, 431–433.
(25) Kraft, B. M.; Jones, W. D. *J. Organomet. Chem.* **2002**, *658*, 132–140.
(26) (a) Edelbach, B. L.; Rahman, A. K. F.; Lachicotte, R. J.; Jones, W. D. *Organometallics* **1999**, *18*, 3170–3177. (b) Doster, M. E.; Johnson, S. A. *Angew. Chem., Int. Ed.* **2009**, *48*, 2185–2187.
(27) Reade, S. P.; Mahon, M. F.; Whittlesey, M. K. *J. Am. Chem. Soc.* **2009**, *131*, 1847–1861.
(28) (a) Harman, W. D. *Top. Organomet. Chem.* **2004**; *7*, 95−127.(b) Harman, W. D. *Coord. Chem. Rev.* **2004**, *248*, 853–866. (c) Begum, R. A.; Sharp, P. R. *Organometallics* **2005**, *24*, 2670–2678.
(29) Braun, T.; Cronin, L.; Higgitt, C. L.; McGrady, J. E.; Perutz, R. N.; Reinhold, M. *New J. Chem.* **2001**, *25*, 19–21.
(30) (a) Erhardt, S.; Macgregor, S. A. *J. Am. Chem. Soc.* **2008**, *130*, 15490–15498. (b) Nova, A.; Erhardt, S.; Jasim, N. A.; Perutz, R. N.; Macgregor, S. A.; McGrady, J. E.; Whitwood, A. C. *J. Am. Chem. Soc.* **2008**, *130*, 15499–15511.

Scheme 3

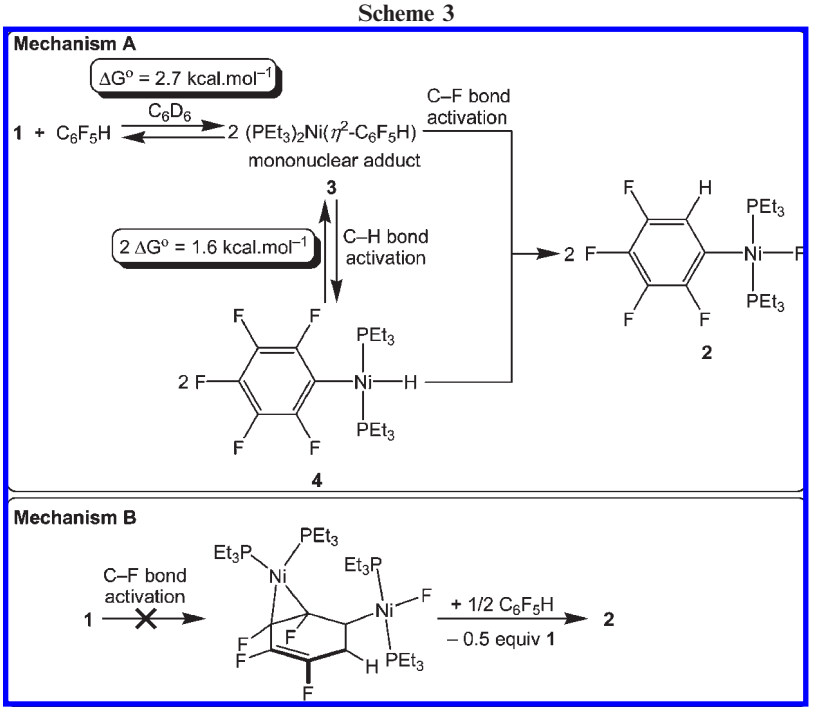

as the mononuclear adduct $(PEt_3)_2Ni(\eta^2\text{-}C_6F_5H)$, **3**. This complex displays a $^{31}P\{^1H\}$ NMR resonance at δ 15.9 and three resonances in the ^{19}F NMR spectrum at δ −138.8, −164.9, and −171.3, with relative integrals of 2:2:1. The resonance at δ −138.8 has a $^3J_{FH}$ of 11.5 Hz, consistent with its identity as the *ortho*-F, which identifies the resonances at δ −164.9 and −171.3 as the *meta*- and *para*-F resonances, respectively. The presence of only three ^{19}F resonances for a solution of **3** in C_7D_8, even as low as 223 K, implies a rapidly fluxional compound where the $(PEt_3)_2Ni$ moiety readily moves between η^2-coordination of adjacent carbon atoms of the π-system with a negligible barrier, consistent with both calculations[7] and experimental precedent[23] for related molecules. The ^1H NMR spectrum is also consistent with this fluxionality and displays a multiplet resonance at δ 5.16 that is a triplet of triplets, with J_{HF} values of 11.4 and 4.9 Hz. Signals for the PEt_3 groups observed at 0.85 and 1.39 were also attributable to mononuclear complex **3**.

DFT calculations were performed on the η^2-isomers of the model complexes $(PH_3)_2Ni(\eta^2\text{-}C_6F_5H)$, **3a**−**c**$^{\mathbf{H}}$, and $(PMe_3)_2Ni(\eta^2\text{-}C_6F_5H)$, **3a**−**c**$^{\mathbf{Me}}$, shown in Scheme 4. These calculations indicate that the isomers **a** and **c**, where the Ni-$(PR_3)_2$ moiety is bound to the 1,2 and 3,4 sites of the aromatic ring, respectively (where the hydrogen bearing carbon is labeled the 1 site), are very close in energy and should both be present at room temperature, whereas the 2,3 isomer **b** should not be present in significant amounts. The calculated ^{19}F NMR shifts for **3a**$^{\mathbf{Me}}$, obtained by averaging the pairs of *ortho* and *meta* environments, are δ −142.6 for the *ortho*-fluorines, δ −168.3 for the *meta*-fluorines, and δ −169.9 for the *para*-fluorine. Surprisingly, the calculated shifts for the **3c**$^{\mathbf{Me}}$ isomer are nearly identical. The *ortho*, *meta*, and *para* fluorine substituents are predicted to display chemical shifts of δ −143.4, −166.7, and −169.2. Both model isomers are in good agreement with the observed shifts. Model **3a**$^{\mathbf{Me}}$ has a maximum error in chemical shifts of 3.9 ppm, whereas model **3c**$^{\mathbf{Me}}$ has a maximum error of 4.6 ppm, compared to the experimentally observed spectrum for **3**. The root-mean-square errors

Scheme 4

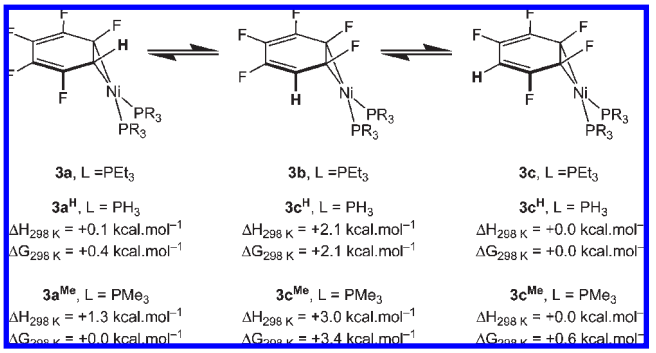

in the predicted shifts are 3.0 and 3.1 ppm for **3a**$^{\mathbf{Me}}$ and **3c**$^{\mathbf{Me}}$, respectively. These results support the assignment of the ^{19}F chemical shifts of **3**, but do not help the assignment if isomer **a** or **c** is predominant in the solution.

The second species observed in the mixtures of **1** and C_6F_5H was an equilibrium amount of hydride **4**, the presence of which was verified by the observation of a broad, barely resolvable triplet resonance in the ^1H NMR spectrum at δ −14.92. In C_7D_8 solutions of **1** and C_6F_5H, this signal sharpens upon cooling to 243 K to reveal a triplet of triplets of triplets with coupling to two equivalent ^{31}P nuclei with a $^2J_{PH}$ value of 68.4 Hz, two equivalent *ortho*-F nuclei with a $^4J_{FH}$ value of 10.5 Hz, and a $^5J_{FH}$ value of 4.7 Hz. This resonance is comparable to the known analogue *trans*-$(PEt_3)_2NiH(2,3,5,6\text{-}C_6F_4H)$,[10] which displays a hydride ^1H NMR resonance at δ −14.3, with a $^2J_{PH}$ value of 67.7 Hz as well as $^4J_{FH}$ and $^5J_{FH}$ constants of 9.5 and 4.2 Hz, respectively. Resonances for hydride **4** were observed in the $^{19}F\{^1H\}$ NMR spectrum at δ −114.1, −162.5, and −163.9 and are comparable to those observed for the known structurally related fluoride *trans*-$(PEt_3)_2NiF(C_6F_5)$, which displays aromatic resonances at δ −115.4, −161.1, and −163.8.[15] Further evidence that the ^{19}F signals observed

Scheme 5

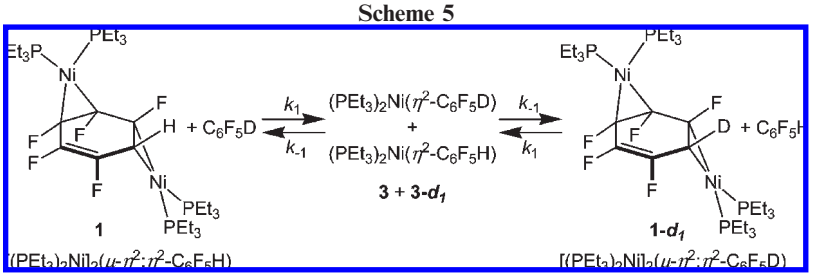

are indeed hydride **4** was obtained by comparing the $^{19}F\{^1H\}$ and ^{19}F NMR spectra. The *ortho*-F multiplet at δ −114.1 displays a $^4J_{FH}$ of 10.5 Hz, and the *meta*-F resonance at δ −163.9 displays a $^5J_{FH}$ of 4.8 Hz, which are both consistent with the coupling constants of the hydride signal observed in the ^1H NMR of **4**. The *para*-F resonance at δ −162.5 is a triplet of triplets with J_{FF} values of 20.0 and 3.6 Hz, but no resolved coupling to the hydride. The $^{31}P\{^1H\}$ resonance associated with **4** was observed at δ 23.4, and its identity was verified by the observation of a $^2J_{PH}$ value of ∼70 Hz in the ^1H-coupled ^{31}P NMR spectrum.

These data can be used to estimate an equilibrium constant for the conversion of **3** to **4** of 0.25(3), which corresponds to a $\Delta G°_{303\,K}$ value of +0.8(1) kcal·mol^{-1} for this conversion. By monitoring reagent concentrations versus the internal standard Ph_3SiF, it was possible to determine an equilibrium constant of 0.011(4) for the equilibrium conversion of the dinuclear complex **1** and C_6F_5H to 2 equiv of the mononuclear complex **2** shown in Scheme 1. The large variation in this number reflects the sensitivity of this equilibrium to the changing C_6F_5H concentration. The equilibrium constant corresponds to a $\Delta G°_{303\,K}$ value of +2.7(2) kcal·mol^{-1} for this conversion. It follows that the $\Delta G°_{303\,K}$ value for the conversion of the dinuclear complex **1** and C_6F_5H to 2 equiv of hydride **4** is +4.3(3) kcal·mol^{-1}.

An experiment where 20 equiv of C_6F_5H was added to a C_7D_8 solution of 20 mg of **1** at low temperatures and then transferred into a NMR probe precooled to 243 K provided evidence that C−H activation is slow at this temperature. Only trace amounts of **4** were observed, and other than **1** and C_6F_5H, the only other significant ^{19}F and $^{31}P\{^1H\}$ NMR resonances observed were those associated with **3**. Warming to 273 K and monitoring by ^{19}F and $^{31}P\{^1H\}$ NMR spectroscopy, the resonances associated with hydride **4** are observed, which indicates that C−H bond activation occurs rapidly well below room temperature.

The observation of species **3** and **4** does not necessarily rule out the possibility of mechanism B as the lowest energy pathway for C−F bond activation, but these mechanisms should be distinguishable by monitoring the effect of added C_6F_5H on the rate of conversion of **1** to **2**, because the rate law derived from mechanism B has no dependence on C_6F_5H concentration. Qualitatively, it is evident that the addition of C_6F_5H accelerates the reaction. In the presence of ∼90 equiv of C_6F_5H, ∼25 mM solutions of **1** in C_6D_6 converts to **2** over the course of approximately 5.5 h at 303 K. Under identical conditions, solutions with ∼20 and 9 equiv of C_6F_5H take ∼17 and 33 h to go to completion, respectively. A solution with 2.8 equiv of C_6F_5H barely reached two half-lives over a 48 h period. It is therefore unlikely that mechanism B contributes significantly to the C−F bond activation pathway, whereas mechanism A appears plausible.

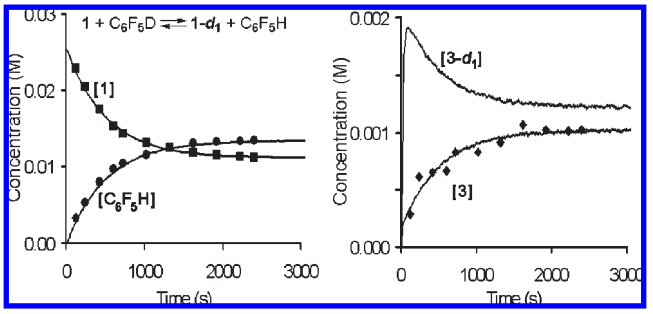

Figure 5. Left: Concentration of **1** and C_6F_5H versus time in the reaction of 1.2 equiv of C_6F_5D with **1** at 303 K. Experimentally determined concentration of **1** and C_6F_5H are shown as boxes and circles, respectively. Lines show the simulated kinetic data. Right: Experimentally determined concentration of **3** versus time. Experimental data points are shown as diamonds, with lines showing simulated kinetics data. Simulated data for the concentration of **3-*d*$_1$** are included for comparison.

The exact rate law for the conversion of **1** to **2** via mechanism A is complicated due to the side-equilibrium with hydride **4** and the potential for either the first step, the formation of mononuclear **3**, or the second step, the conversion of **3** to **2**, to be rate determining. It proved possible to examine the rate of the initial equilibrium formation of the mononuclear complex **3** via the reaction of **1** with C_6F_5D, as shown in Scheme 5.

This equilibration was studied using a 0.028 M solution of **1** in C_6D_6, with 1.2 equiv of added C_6F_5D. The progress of the reaction was followed by monitoring the decrease in the concentration of **1** and the appearance of C_6F_5H by ^1H NMR spectroscopy at 303 K. Equilibrium was reached within 40 min. An initial model for the rate of equilibration was performed with the rates of all four permutations of the conversion between **1**/**1-*d*$_1$** and C_6F_5H/C_6F_5D to **3**/**3-*d*$_1$** assumed identical. The equilibrium constant for the reaction of 0.07 was determined from the ^1H NMR spectrum and was assumed to be unchanged by secondary isotope effects. The rates k_1 and k_{-1} were determined to be 0.070 and 10 $M^{-1}\cdot s^{-1}$, respectively, from this preliminary analysis. This model provided an excellent fit for the concentration of **1** and C_6F_5H versus time, but failed to accurately predict the concentration of **3** versus time. With these rate constants, it can be shown that the initial concentrations of **3** and **3-*d*$_1$** should be nearly equivalent and increase steadily for ∼100 s according to this model. The slight conversion to equilibrium concentrations of **3** and **3-*d*$_1$** then occurs gradually. The experimental concentration of **3** versus time is shown on the right of Figure 5 and does not fit this model, as it continually increases as C_6F_5H is liberated. A second model was tested with an additional equilibrium reaction that could interconvert **3** and C_6F_5D to **3-*d*$_1$** and C_6F_5H. If this reaction was treated as being significantly faster than the conversions

of **1**/**1-d_1** and C_6F_5H/C_6F_5D to **3**/**3-d_1**, the rate constants k_1 and k_{-1} were determined to be 0.04 and 5.7 $M^{-1}\cdot s^{-1}$, respectively. The lowest rate constant for the conversion of **3** and C_6F_5D to **3-d_1** and C_6F_5H that was found to fit the observed concentration of **3** was 5 $M^{-1}\cdot s^{-1}$, with the reverse reaction assumed to occur at the same rate; a larger rate constant cannot be ruled out, but does not significantly affect the result of the simulation. The simulated lines[31] and experimental data points from this model are shown in Figure 5.

The product distribution after conversion of this mixture to **2** and **2-d_1** provided further insight into the C−F activation reaction mechanism. The ratio of **2** to **2-d_1** formed can be determined from integration of the ^{19}F NMR signal of the F nucleus in the 5-position of the aromatic ring, adjacent to the H/D nucleus. The resonance at −142.7 for **2** is accompanied by a resonance at −143.0 for **2-d_1**, which are similar in intensity. A mechanism where the hydride **4** is an immediate precursor to the C−F bond activation transition state therefore seems unlikely, as a primary kinetic isotope effect should significantly favor **4** over **4-d_1**.[10] However, it is impossible from this data to rule out a smaller secondary isotope effect in this reaction.

The C−F bond activation that forms **2** is considerably slower than the rate of formation of **3**, so the formation of the mononuclear complex is not rate determining under most reaction conditions. However, the rapid rate at which both **1** and **3** transfer to $Ni(PEt_3)_2$ fragments to C_6F_5H raises questions regarding the nature of the reaction mechanism. It is not clear whether the expected mechanism, in which **3** converts from a π-bound ground state to a transition state with the *ortho* C−F bond σ-bound to the $Ni(PEt_3)_2$ moiety, must occur in an intramolecular fashion[7] or if both intramolecular and intermolecular pathways are accessible to produce the intermediate to the C−F activation product **2**. Attempts to model the reaction kinetics of the conversion of **1** to **2** in the presence of excess C_6F_5H were made, but the observed reaction kinetics proved poorly reproducible, with spectroscopically identical samples of **1** resulting in moderately different reaction rates.

Synthesis of a Dinuclear $Ni(PEt_3)_2$ Adduct of C_6F_6. Previous reports of the activation of C_6F_6 with $Ni(PEt_3)_2$ precursors failed to observe any intermediates.[14,15] However, similar to the synthesis of **1**, the reaction of the anthracene adduct $(PEt_3)_2Ni(\eta^2\text{-}C_{14}H_{10})$ with C_6F_6 in pentane proceeds immediately, with a color change from red to yellow and the precipitation of anthracene to produce $[(PEt_3)_2Ni]_2(\mu\text{-}\eta^2{:}\eta^2\text{-}C_6F_6)$, **5**, as shown in eq 3. Unlike the reaction of $(PEt_3)_2Ni(\eta^2\text{-}C_{14}H_{10})$ with C_6F_5H, there is no indication that this reaction is in equilibrium, presumably due to the enhanced electron-accepting ability of C_6F_6, and this reaction occurs readily with a stoichiometric quantity of C_6F_6.

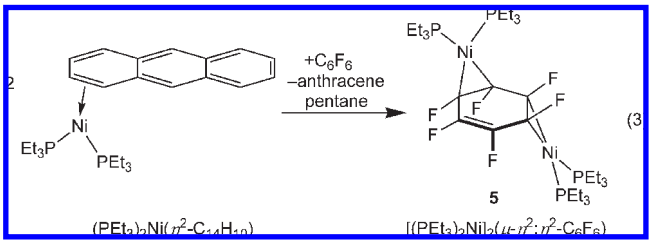

(31) Hinsberg, W.; Houle, F.; Allen, F.; Yoon, E. *Chemical Kinetics Simulator 1.01*; International Business Machines Corporation, **1996**.

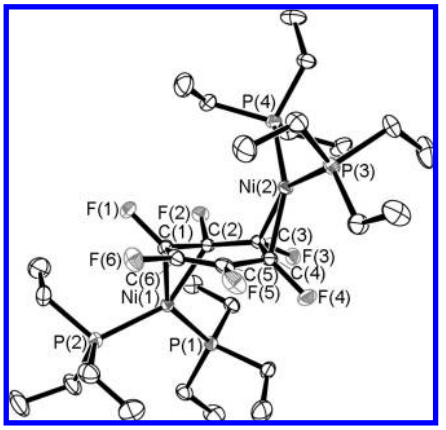

Figure 6. ORTEP depiction of the solid-state molecular structure of **5** as determined by X-ray crystallography. Hydrogen atoms are omitted for clarity. The 30% probability ellipsoids are shown. Selected bond lengths (Å): C(1)−C(2) 1.438(3); C(2)−C(3), 1.460(3); C(3)−C(4), 1.436(3); C(4)−C(5), 1.451(4); C(5)−C(6), 1.323(4); C(6)−C(1), 1.448(4); Ni(1)−C(1), 1.910(2); Ni(1)−C(2), 1.953(2); Ni(1)−P(2), 2.1827(7); Ni(1)−P(1), 2.1853(7); Ni(2)−C(4), 1.907(2); Ni(2)−C(3), 1.953(2);Ni(2)−P(3), 2.1791(7); Ni(2)−P(4), 2.1821(7). Selected angles (deg): P(2)−Ni(1)−P(1) 113.87(3); P(3)−Ni(2)−P(4), 110.36(3).

Crystals suitable for characterization by X-ray crystallography were obtained by cooling a pentane solution of **5** to −40 °C, and an ORTEP depiction of the solid-state molecular structure is shown in Figure 6. The unit cell parameters for **5** are nearly identical to those observed for **1**, and the gross structural details are also similar. The structure of **5** features greater distortions in the Ni bonding to the aromatic rings than was observed in **1**. The Ni(1)−C(2) and Ni(2)−C(3) bond lengths in **5** are both 1.953(2) Å, similar to the analogous bond lengths in **1**; however, the Ni(1)−C(1) and Ni(2)−C(4) bond lengths of 1.910(2) and 1.907(2) Å, respectively, are significantly shorter than the related bond lengths in **1** of 1.935(3) and 1.957(3) Å. The C−C bond distances of the C_6F_6 ring are altered from their aromatic lengths in a manner similar to that observed in **1**, with the C(5)−C(6) bond length of 1.323(4) Å indicative of a double bond.

Variable-Temperature ^{19}F and ^{31}P NMR Spectroscopy. Complex **5** exhibits a very broad pair of overlapping peaks in the 282.5 MHz room-temperature ^{19}F NMR spectrum. These broad ^{19}F resonances span from approximately δ −60 to −130, indicative of fluxionality. The experimental variable-temperature ^{19}F NMR spectra from 190 to 330 K are shown in Figure 7. The slow-exchange limit spectrum obtained at 190 K displays three fluorine environments, as anticipated for a C_2 symmetric species, with two peaks nearly coincidental at δ −158.0 and a third peak at δ −195.0. The nearly coincident peaks coalesce upon warming to 220 K, but coalescence of the third resonance at δ −195.0 does not occur until room temperature. This fluxional process is presumably analogous to that proposed for complex **1** and thus involves 1,3-shifts of the $(PEt_3)_2Ni$ moieties around the C_6F_6 ring. Unlike complex **1**, these shifts exchange all the ^{19}F nuclei environments, and modeled variable-temperature spectra are shown on the right-hand side of Figure 7. The activation barrier can be estimated as 12.3 kcal·mol^{-1} using the Arrhenius equation, or alternatively, the temperature dependence of the rate of exchange can be fit using the Eyring equation, which provides a $\Delta H^{\ddagger}$ value of 11.8 kcal·mol^{-1}

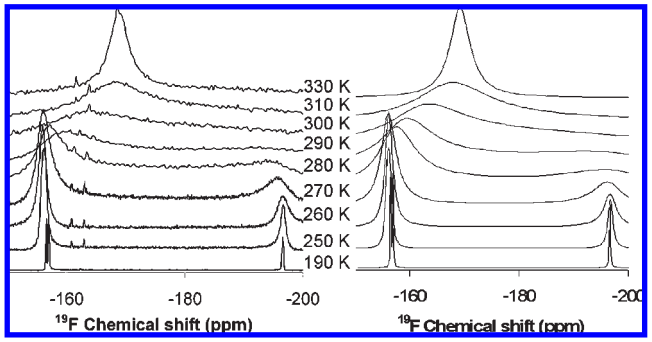

Figure 7. Experimental (left) and modeled (right) variable-temperature ^{19}F NMR spectra for complex **5**, obtained at 282.4 MHz.

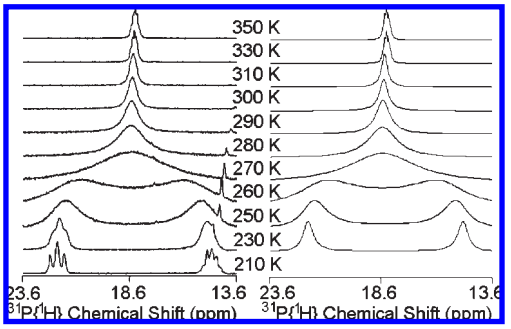

Figure 8. Experimental (left) and modeled (right) variable-temperature $^{31}P\{^1H\}$ NMR spectra for complex **5** obtained at 121.5 MHz.

with a small contribution from $\Delta S^{\ddagger}$ of 1.0 cal·mol^{-1}. These values are slightly larger than the barrier of 10 kcal·mol^{-1} determined for the interconversion of **1a** and **1c**.

To further test our previous assumption that DFT calculations could be used to determine the ^{19}F NMR shifts in these dinuclear adducts, attempts were made to model the shifts observed in **5**. The calculated ^{19}F chemical shifts for **5** using the model complex $[(PH_3)_2Ni]_2(\mu\text{-}\eta^2\text{:}\eta^2\text{-}C_6F_6)$ were found to be δ −156.4, −161.4, and −187.8, and changing the phosphine donor to the significantly stronger PMe_3 donor in the model complex $[(PMe_3)_2Ni]_2(\mu\text{-}\eta^2\text{:}\eta^2\text{-}C_6F_6)$ resulted in only slightly different predicted shifts of δ −156.9, −160.7, and −191.0, which is in excellent agreement with the experimentally observed shifts of δ −158.0, −158.0 (nearly coincidental) and −195.0, with a maximum error of 4.0 ppm and a root-mean-square error of 2.9 ppm. This prediction also allows the identification of the resonance at δ −195.0 in **5** as corresponding to F(1) and F(4), from the labeling scheme used in Figure 6.

Variable-temperature 121.5 MHz $^{31}P\{^1H\}$ NMR spectra were also obtained for **5** and are shown in Figure 8. Complex **5** displays a single broad resonance in the room-temperature $^{31}P\{^1H\}$ NMR spectrum at δ 18.9. At 350 K a fast-exchange limit $^{31}P\{^1H\}$ NMR spectrum could be obtained, despite the fact that **5** rapidly converts to the C−F activation product, a metallic nickel precipitate, and other unidentified products at this temperature. The resonance for **5** is a septet at δ 18.3 due to coupling of the exchange-averaged phosphorus environments to six equivalent fluorine nuclei, with an observed J_{FP} of 8.8 Hz. Cooling a room-temperature solution leads to decoalescence at 260 K, and two multiplets are observed at 210 K. These spectra were modeled, as shown on the right-hand side of Figure 8, and the rates of exchange determined from these spectra were used to estimate the barrier to phosphine exchange. The Arrhenius activation energy of 11.5 kcal·mol^{-1} is similar to the value determined from the variable-temperature ^{19}F NMR spectra. Likewise the Eyring equation can be used to calculate a $\Delta H^{\ddagger}$ value of 10.9 kcal·mol^{-1} with a small contribution from $\Delta S^{\ddagger}$ of −2.6 cal·mol^{-1}.

C−F Bond Activation in Complex 5. Similar to complex **1**, complex **5** undergoes C−F bond activation at room temperature, but in the absence of added C_6F_6 this reaction proceeds with a dark precipitate of metallic nickel and numerous impurities. In the presence of added C_6F_6, this reaction occurs cleanly to yield the known C−F bond activation product *trans*-$(PEt_3)_2NiF(C_6F_5)$,[14,15] which is observed as a doublet in the $^{31}P\{^1H\}$ NMR spectrum at δ 12.2 ($^2J_{PF}$ = 48 Hz). In the presence of added C_6F_6, a single new resonance was observed in the ^{19}F NMR spectra, which could be attributed to a small equilibrium amount of the fluxional mononuclear complex $(PEt_3)_2Ni(\eta^2\text{-}C_6F_6)$, **6**, at δ −167.4, and a resonance in the $^{31}P\{^1H\}$ NMR was observed at δ 17.0. The latter appeared to be a multiplet, but the coupling could not be adequately resolved to unambiguously assign this complex.

Intermediates in the Reaction of C_6F_6 and C_6F_5H with Ni$(PEt_3)_4$. Previous reports[14,15] of C−F bond activation in both C_6F_6 using $Ni(PEt_3)_4$ or $(PEt_3)_2Ni$(1,5-cyclooctadiene) gave no indication of intermediates via NMR analysis; however, in consideration of the broad peaks observed in the ^{19}F and $^{31}P\{^1H\}$ spectra of **5** we decided to re-examine this reaction. Immediately upon mixing a purple C_6D_6 solution of $Ni(PEt_3)_4$ with C_6F_6, the solution turned yellow, which implies a reaction has taken place, although the C−F bond activation reaction takes weeks at room temperature. The ^{19}F and $^{31}P\{^1H\}$ NMR spectra both reveal the resonances observed for **5**.

The analogous addition of C_6F_5H to $Ni(PEt_3)_4$ resulted in a color change from purple to yellow and the observation of the adduct **1** by ^{19}F and $^{31}P\{^1H\}$ NMR spectroscopy. The resonances associated with **3** and **4** were also observable in the ^{19}F spectrum. This reaction was previously reported to give a mixture that included multiple C−F bond activation products, presumed to be due to unselective activation of the *ortho*-, *meta*-, and *para*-F environments. Under these conditions, the reaction proceeded to provide four C−F activation products, as shown in Scheme 6. Unexpectedly, the major product (65%) is not the *ortho* activation product **2**, but rather the *para* activation product $(PEt_3)_2NiF(2,3,5,6\text{-}C_6F_4H)$ (**7**), with a $^{31}P\{^1H\}$ NMR resonance at δ 13.6 (d, J_{PF} = 45.6 Hz) and ^{19}F NMR resonances at δ −117.5, −141.9, and −387.3, which is consistent with previous characterization.[10] The second most prevalent C−F activation product (22%) is due to activation at the *meta* site, $(PEt_3)_2NiF(2,3,4,6\text{-}C_6F_4H)$ (**8**), and displays ^{19}F NMR resonances at δ −91.0, −110.1, −142.1, −168.4, and −387.6 and a $^{31}P\{^1H\}$ resonance at δ 13.2 (d, J_{PF} = 47.4 Hz). Confirmation of this assignment was aided by the prediction of the ^{19}F NMR shifts for the model complex $(PH_3)_2NiF(2,3,4,6\text{-}C_6F_4H)$, $\mathbf{9^H}$, using DFT calculations, which yielded calculated shifts of δ −97.0, −112.9, −141.2, and −169.4 for the 6, 2, 4, and 3 sites, respectively. The *ortho*-F activation product **2** was a minor product (12%) in this mixture, with ^{19}F NMR resonances at δ −116.6, −142.4, −159.8, −165.7, and −380.3 and a $^{31}P\{^1H\}$ NMR resonance at δ 12.5 (d, J_{PF} = 44.7 Hz). Trace amounts of the previously reported product of C_6F_6

Scheme 6

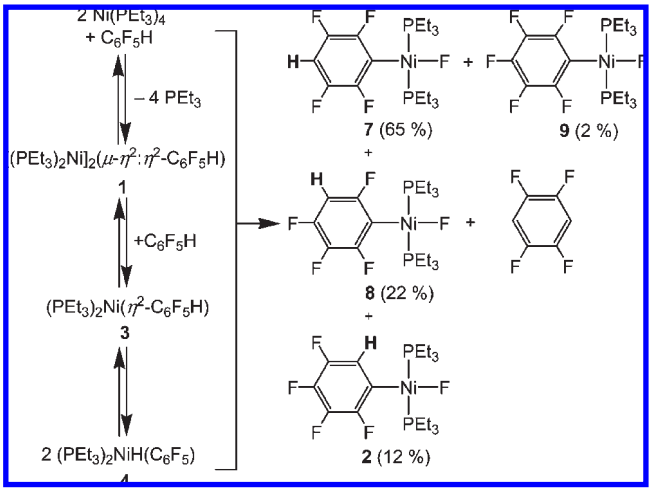

activation (2%), $(PEt_3)_2NiF(C_6F_5)$ (**9**), were also observed at δ −115.5, −161.2, and −163.9, along with some 1,2,4,5-tetrafluorobenzene at δ −139.5. These trace products formally represent a hydrodefluorination reaction, as we have previously reported with 1,2,4,5-tetrafluorobenzene. Although it is possible that this reaction occurs by a transmetalation reaction involving the intermediate hydride **4**, we cannot rule out alternate mechanisms, such as electron transfer[16] from $Ni(PEt_3)_4$ to provide an intermediate anionic fluoroaromatic radical, $C_6F_5H^{\bullet -}$, which could lose F^- to generate the $C_6F_4H^{\bullet}$ radical. This radical could then abstract $H^{\bullet}$ from C_6F_5H to provide 1,2,4,5-tetrafluorobenzene and the $C_6F_5^{\bullet}$ fragment, which could then combine with the Ni(I) species generated from electron transfer and the F^- moiety to form $(PEt_3)_2NiF(C_6F_5)$. Irrespective of the mechanisms involved in the production of these various C−F activation products, it is apparent that the C−F bond activation of C_6F_5H with $Ni(PEt_3)_4$ does not proceed in a selective manner, despite the observation of the same intermediates observed in the selective conversion of **1** to **2**.

An improvement in selectivity using $Ni(PEt_3)_4$ could be achieved by using an excess of C_6F_5H. With 20 equiv the major C−F activation product was found to be **2** (67%), with **7** (27%) and **8** (6%) observed as minor products. This observation is consistent with more than one operating reaction mechanism in this system, with the activation from the mechanism adopted by **1** increasingly prevalent with added C_6F_5H.

DFT Calculations. These experimental results demonstrate that in the presence of excess arene the antifacial dinuclear bis-$(PEt_3)_2Ni$ adducts of both C_6F_5H and C_6F_6 convert to mononuclear adducts, as well as a C−H activation product in the case of C_6F_5H. We sought to investigate these interconversions by DFT, to gauge the importance of phosphine donor and fluoroaromatic in the thermodynamic preference for dinuclear adduct, mononononuclear adduct, or C−H activation in these systems.

The reaction of the dinuclear C_6F_6 adducts $[(PR_3)_2Ni]_2$-$(\mu$-η^2:η^2-$C_6F_6)$ with C_6F_6 to produce the mononuclear complexes $(PR_3)_2Ni(\eta^2$-$C_6F_6)$ was examined for phosphine donors PH_3 ($\mathbf{5^H}$, $\mathbf{6^H}$), PMe_3 ($\mathbf{5^{Me}}$, $\mathbf{6^{Me}}$), and PEt_3 (**5, 6**), as shown in Scheme 7. The enthalpy change for these reactions is slightly unfavorable; however the value decreases with the larger and more electron-donating phosphines, with enthalpy changes of 10.1, 8.0, and 7.1 kcal·mol^{-1} for PH_3, PMe_3, and PEt_3 donors, respectively. The Gibbs free energy changes are all slightly lower that the enthalpy changes, though the $\Delta G_{298\,K}$ value for PMe_3 is inexplicably lower than that of PEt_3.

Scheme 7

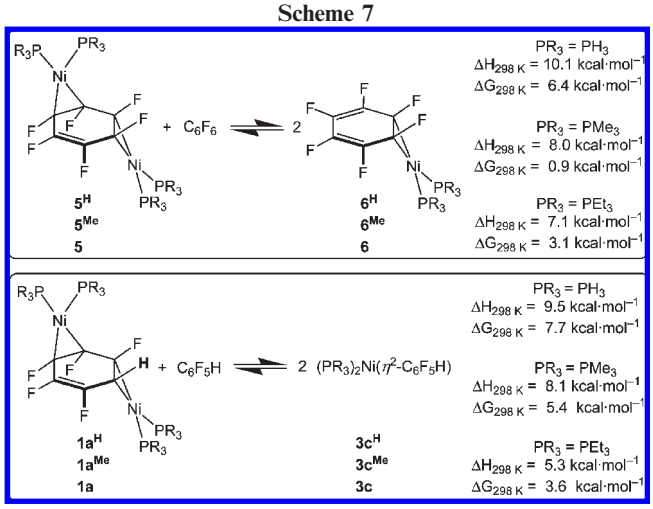

Scheme 8

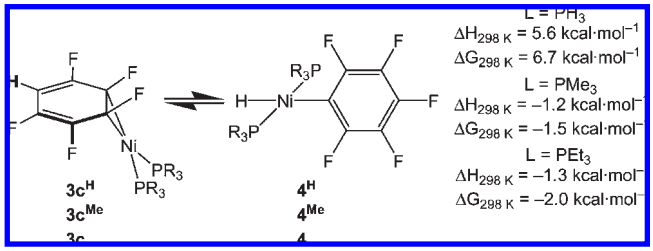

The lower transformation in Scheme 7 displays the analogous equilibrium between $[(PR_3)_2Ni]_2(\mu$-η^2:η^2-$C_6F_5H)$ and C_6F_5H to produce the mononuclear complexes $(PR_3)_2Ni$-$(\eta^2$-$C_6F_5H)C_6F_5H$, which was examined for phosphine donors PH_3 ($\mathbf{1a^H}$, $\mathbf{3c^H}$), PMe_3 ($\mathbf{1a^{Me}}$, $\mathbf{3c^{Me}}$), and PEt_3 (**1**, **3**). A similar trend is observed with the enthalpy changes, which are 9.5, 8.1, and 5.3 kcal·mol^{-1} for PH_3, PMe_3, and PEt_3 donors, respectively; however, the Gibbs free energy change for the conversion also drops steadily in this series from 7.7 kcal·mol^{-1} for conversion of $\mathbf{1a^H}$ to $\mathbf{3c^H}$ to 3.6 kcal·mol^{-1} for the conversion of **1a** to **3c**. This latter calculated Gibbs free energy change for these species in the gas phase is close to that estimated from the experimentally determined value in C_6D_6 of +2.7 kcal·mol^{-1}.

Calculations of the influence of phosphine donor on the thermodynamics of the C−H bond activation step that converts the mononuclear complex $(PR_3)_2Ni(\eta^2$-$C_6F_5H)$ **3c** to hydride **4** were also carried out, using the PH_3, PMe_3, and PEt_3 donors and the same labeling convention, as shown in Scheme 8. The donor ability of the phosphine has a large influence on this reaction, with the oxidative addition enthalpically disfavored by 5.6 kcal·mol^{-1} for the weaker PH_3 donor and enthalpically favored by −1.2 and −1.3 kcal·mol^{-1} for the complexes with the stronger PMe_3 and PEt_3 donors, respectively. A similar trend is observed for the Gibbs free energy values for these transformations. This reflects the propensity for a more electron rich metal center to undergo oxidative addition. Surprisingly, the differences between the values calculated for the PMe_3 and PEt_3 donors are negligible. The calculated value for the conversion of **3** to

4 of -2.0 kcal·mol^{-1} is slightly in error compared to the experimentally determined value of 0.8 kcal·mol^{-1}, which may be due to the increased entropy of **3** due to the presence of alternate isomers with nearly identical energies, but may also reflect the errors associated with gas-phase rather than solution DFT calculations.

Conclusions

Although the C−F bond activation of C_6F_6 by $Ni(PEt_3)_4$ has been known for over thirty years,[14] little insight has been obtained into the mechanism of this reaction or of the analogous previously reported unselective activation of C_6F_5H.[15] Despite the apparent similarity as a source of the $(PEt_3)_2Ni$ moiety, the reaction of the anthracene adduct $(PEt_3)_2Ni(\eta^2\text{-}C_{14}H_{10})$ with pentafluorobenzene produces an isolable dinuclear adduct, which is slightly thermodynamically favored over the mononuclear adduct. Reaction with excess C_6F_5H provided an equilibrium amount of the mononuclear arene adduct as well as the C−H activation product. These mixtures ultimately undergo C−F activation at the *ortho*-F with >97% selectivity. This selectivity is unique to this system, which may prove useful in the functionalization of partially fluorinated aromatic compounds. Mechanistic studies show that hopping of the $Ni(PEt_3)_2$ moiety between C_6F_5H rings is more rapid than C−F bond activation and that the commonly accepted intramolecular mechanism of C−F bond activation may not be true.

A reinvestigation of the reaction of C_6F_5H with $Ni(PEt_3)_4$ revealed the same dinuclear, mononuclear, and C−H activation intermediates observed with $(PEt_3)_2Ni(\eta^2\text{-}C_{14}H_{10})$, but further reaction proceeded to a mixture of C−F activation products, with activation at the *para*- and *meta*-F providing the major products. Radical intermediates appear likely in these reactions and may explain some previously reported byproduct in the activation of 1,2,4,5-tetrafluorobenzene.[10]

These mechanistic studies point to a significantly more complex mechanism of C−F activation in these reactions than has previously been anticipated and also demonstrate the viability of nickel phosphine complexes in selective activation and functionalization of both C−F and C−H bonds[10,32] of fluorinated aromatics.

Experimental Section

General Procedures. Unless otherwise stated, all manipulations were performed under an inert atmosphere of nitrogen using either standard Schlenk techniques or an MBraun glovebox. Dry, oxygen-free solvents were employed throughout. Anhydrous pentane was purchased from Aldrich, sparged with dinitrogen, and passed through activated alumina under a positive pressure of nitrogen gas and further deoxygenated using Ridox catalyst columns.[33] Deuterated benzene was dried by heating at reflux with sodium/potassium alloy in a sealed vessel under partial pressure, then trap-to-trap distilled, and freeze−pump−thaw degassed three times. Deuterated toluene was purified in an analogous manner by heating at reflux over Na. NMR spectra were recorded on a Bruker AMX (300 MHz) or Bruker AMX (500 MHz) spectrometer. All chemical shifts are reported in ppm, and all coupling constants are in Hz. For $^{19}F\{^1H\}$ NMR spectra, $CFCl_3$ in $CDCl_3$ was used as the external reference at δ 0.00. ^1H NMR spectra were referenced to residual protons (C_6D_5H, δ 7.15; C_7D_7H, δ 2.09) with respect to tetramethylsilane at δ 0.00. $^{31}P\{^1H\}$ NMR spectra were referenced to external 85% H_3PO_4 at δ 0.0. $^{13}C\{^1H\}$ spectra were referenced relative to solvent resonances (C_6D_6, δ 128.0; C_7D_8, δ 20.4). Elemental analyses were performed by the Centre for Catalysis and Materials Research (CCMR), Windsor, Ontario, Canada. The compounds $(PEt_3)_2Ni(\eta^2\text{-}C_{14}H_{10})$[17] and $Ni(PEt_3)_4$[34] were prepared by literature procedures. The compounds C_6F_5H, C_6F_6, and C_6F_5Br were purchased from Aldrich, degassed, and dried over molecular sieves prior to use.

Synthesis of $[(PEt_3)_2Ni]_2(\mu\text{-}\eta^2\text{:}\eta^2\text{-}C_6F_5H)$ (1). To a stirred solution of the anthracene adduct $(PEt_3)_2Ni(\eta^2\text{-}C_{14}H_{10})$ (1.00 g, 2.11 mmol) in 5 mL of pentane was added 0.5 mL (4.5 mmol) of C_6F_5H. The reaction mixture immediately turned from dark red to orange, and anthracene precipitated from solution over the course of 5 min. The mixture was then immediately filtered through Celite and cooled to −40 °C; if the solution is left for an excessive time at room temperature, **2** is produced as a byproduct. The resultant yellow crystals were isolated by filtration and dried under vacuum (yield 0.56 g, 70%). ^1H NMR (C_6D_6, 300 MHz, 298 K): δ 1.01 (m, 36H, PCH_2CH_3), 1.61 (m, 24H, PCH_2CH_3), 3.12 (m, 1H, C_6F_5H). ^{19}F NMR (C_6D_6, 282.4 MHz, 298 K): δ −134.9 (br, 1F, $W_{1/2}$ = 114 Hz), −144.0 (br, 1F 1F, $W_{1/2}$ = 132 Hz), −155.2 (br, 1F, $W_{1/2}$ = 153 Hz), −158.7 (br, 1F, $W_{1/2}$ = 107 Hz), −185.4 (br, 1F, $W_{1/2}$ = 115 Hz). $^{31}P\{^1H\}$ NMR (C_6D_6, 121.5 MHz, 298 K): δ 18.5 (br and asymmetric, $W_{1/2}$ = 870 Hz). Anal. Calcd for $C_{30}H_{61}F_5Ni_2P_4$ (MW 758.08): C, 47.53; H, 8.11. Found: C, 47.63; H, 8.09.

Synthesis of $(PEt_3)_2NiF(2,3,4,5\text{-}C_6F_4H)$ (2). A pentane solution of $[(PEt_3)_2Ni]_2(\mu\text{-}\eta^2\text{:}\eta^2\text{-}C_6F_5H)$ (1.02 g, 1.34 mmol) with added C_6F_5H (0.5 mL, 4.5 mmol) was left at room temperature for 1 week. The sample was crystallized by slow evaporation and dried under vacuum (yield 1.14 g, 91%). The assignments of the ^{19}F NMR coupling constants were made with the aid of the $^{19}F\{^1H\}$ spectrum and Gaussian enhancement. ^1H NMR (C_6D_6, 300 MHz, 298 K): δ 0.96 (m, 18H, PCH_2CH_3), 1.08 (m, 12H, PCH_2CH_3), 6.89 (m, 1H, C_6F_5H) . ^{19}F NMR (C_6D_6, 282.4 MHz, 298 K): δ −116.9 (ddddt, 1F, J_{FF} = 31.2, 14.2, 11.0, 0.9 Hz, J_{PF} = 2.6 Hz, *ortho-2-F*), −142.7 (dddt, 1F, J_{FF} = 20.3, 14.2 Hz, J_{FH} = 9.7 Hz, J_{PF} = 2.5 Hz, *ortho* to H *5-F*), −160.2 (ddddt, 1F, J_{FF} = 31.2 19.2, 1.6 Hz, J_{FH} = 2.7 Hz, J_{PF} = 2.8 Hz, *3-F*), −166.1 (ddddt, 1F, J_{FF} = 20.3, 19.2, 1.0 Hz, J_{FH} = 8.6 Hz, J_{PF} = 4.1 Hz, *4-F*), −380.7 (dtm, 1F, J_{FF} = 11.0 Hz, J_{PF} = 47.6 Hz, Ni-*F*). $^{31}P\{^1H\}$ NMR (C_6D_6, 121.5 MHz, 298 K): δ 12.5 (dm, $^2J_{PF}$ = 47.6 Hz). Anal. Calcd for $C_{18}H_{31}F_5NiP_2$ (MW 463.07): C, 56.44; H, 7.64. Found: C, 56.10; H, 7.87.

NMR Spectroscopic Characterization of $(PEt_3)_2Ni(\eta^2\text{-}C_6F_5H)$ (3). To solutions of **1** in C_6D_6 were added 0.5 to 90 equiv of C_6F_5H. In each case an equilibrium amount of **3** was produced. ^1H NMR (C_6D_6, 300 MHz, 298 K): δ 0.85 (m, 18H, PCH_2CH_3), 1.39 (m, 12H, PCH_2CH_3), 5.16 (tt, 1H, J_{HF} = 11.4, 4.9 Hz, C_6F_5H). ^{19}F NMR (C_6D_6, 282.4 MHz, 298 K): δ −138.8 (d of second order m, 2F, $^3J_{FH}$ = 11.5 Hz, *ortho-F*), −164.9 (second order m, 2F, *meta-F*), and −171.3 (m, 1F, *para-F*). $^{31}P\{^1H\}$ NMR (C_6D_6, 121.5 MHz, 298 K): δ 15.9 (s).

NMR Spectroscopic Characterization of $(PEt_3)_2Ni(\eta^2\text{-}C_6F_5H)$ (4). To solutions of **1** in C_6D_6 were added 0.5 to 90 equiv of C_6F_5H. In each case an equilibrium amount of **4** was produced. ^1H NMR (C_6D_6, 300 MHz, 298 K): δ −14.92 (br, Ni-*H*). ^1H NMR (C_6D_6, 300 MHz, 243 K): δ −14.92 (ttt, $^2J_{PH}$ = 68.4 Hz, $^4J_{FH}$ = 10.5 Hz, $^5J_{FH}$ = 4.7 Hz, Ni-*H*). ^{19}F NMR (C_6D_6, 282.4 MHz, 298 K): δ −114.1 (d of second order m, 2F, $^4J_{FH}$ = 10.5 Hz, *ortho-F*), −162.5 (m, 1F, *para-F*), and −163.9 (second order m, 2F, $^5J_{FH}$ = 4.8 Hz *meta-F*). $^{31}P\{^1H\}$ NMR (C_6D_6, 121.5 MHz, 243 K): δ 23.4 (s). ^{31}P NMR (C_6D_6, 121.5 MHz, 243 K): δ 23.4 (d, $^2J \approx 70$ Hz).

(32) Nakao, Y.; Kashihara, N.; Kanyiva, K. S.; Hiyama, T. *J. Am. Chem. Soc.* **2008**, *130*, 16170–16171.
(33) Pangborn, A. B.; Giardello, M. A.; Grubbs, R. H.; Rosen, R. K.; Timmers, F. J. *Organometallics* **1996**, *15*, 1518–1520.
(34) Cundy, C. S. *J. Organomet. Chem.* **1974**, *69*, 305–310.

Synthesis of C_6F_5D. A three-neck round-bottom flask equipped with a water-cooled condenser was charged with Mg (2.734 g, 0.1125 mol, 1.5 equiv) and 80 mL of ether. Neat C_6F_5Br (10.0 mL, 22.0 g, 0.0750 mol) was added in an initial 3 mL aliquot to initiate the reaction, followed by slow dropwise addition via syringe. The solution was stirred for 1 h and then quenched by addition of D_2O (7 mL, 5 equiv). The ether layer was separated and dried with $MgSO_4$ in the ambient atmosphere, and the ether was removed on a benchtop rotary evaporator. The remaining oil was distilled under N_2 at a pressure slightly higher than 1 atm at 98−102 °C. Yield (9.7 g, 76%). The product had no ^{1}H NMR resonances. ^{19}F NMR (C_6D_6, 282.4 MHz, 298 K): δ −139.8 (second order m, 2F, *ortho*-F), −154.5 (t, J_{FF} = 20.8 Hz, 1F, *para*-F), −162.7 (second order m, 2F, *meta*-F).

Reaction of 1 with C_6F_5D. A C_6D_6 solution of **1** (0.0255 M) and C_6F_5D (0.0305 M) was transferred frozen into a NMR probe preheated to 303 K. The rate of exchange was monitored by integration of the resonances associated with C_6F_5H, **1**, and **3** using ^{1}H NMR spectroscopy.

Synthesis of $[(PEt_3)_2Ni]_2(\mu\text{-}\eta^2\text{:}\eta^2\text{-}C_6F_6)$ (5). To a stirred solution of the anthracene adduct $(PEt_3)_2Ni(\eta^2\text{-}C_{14}H_{10})$ (1.00 g, 2.11 mmol) in 5 mL of pentane was added C_6F_6 (0.12 mL, 0.5 equiv). The reaction mixture immediately turned from dark red to yellow and anthracene precipitated from solution. The mixture was filtered through Celite and cooled to −40 °C. The resultant yellow crystals were isolated by filtration and dried under vacuum (yield 0.69 g, 84%). ^{1}H NMR (C_6D_6, 300 MHz, 298 K): δ 0.99 (m, 36H, PCH_2CH_3), 1.61 (m, 24H, PCH_2CH_3). ^{19}F NMR (C_6D_6, 282.4 MHz, 298 K): δ −170 (br and asymmetric, $W_{1/2}$ = ∼6000 Hz). $^{31}P\{^1H\}$ NMR (C_6D_6, 121.5 MHz, 298 K): δ 18.8 (br s). ^{19}F NMR (C_6D_6, 282.4 MHz, 220 K): δ −156.1, −156.2 (second order AB m), −196.5 (m). $^{31}P\{^1H\}$ NMR (C_6D_6, 121.5 MHz, 190 K): δ 15.2 (m), 21.3 (dd, $^3J_{PP}$ = 32 Hz, $^3J_{FP}$ = 32 Hz). Anal. Calcd for $C_{30}H_{60}F_6Ni_2P_4$ (MW 776.07): C, 46.43; H, 7.79. Found: C, 46.52; H, 7.81.

NMR-Scale Reaction of $Ni(PEt_3)_4$ with C_6F_6. To a solution of $Ni(PEt_3)_4$ (42 mg, 0.079 mmol) in C_6D_6 was added C_6F_6 (15 mg, 0.080 mmol). The mixture immediately turned from purple to yellow. The reaction was monitored immediately by ^{19}F NMR spectroscopy, which revealed the presence of **5** and C_6F_6.

NMR-Scale Reaction of $Ni(PEt_3)_4$ with C_6F_5H. To a solution of $Ni(PEt_3)_4$ (42 mg, 0.0790 mmol) in C_6D_6 was added C_6F_6 (14 mg, 0.083 mmol). The reaction was monitored immediately by ^{19}F NMR spectroscopy, which revealed the presence of **1** and C_6F_5H, along with trace equilibrium amounts of **3** and **4**. The reaction proceeded to provide a mixture of C−F activation products over the course of weeks. ^{19}F NMR (C_6D_6, 282.4 MHz, 298 K): major product (**7**) δ −117.5 (m, 2F, *ortho-F*), −141.9 (m, 2F, *meta-F*), −387.3 (m, 1F, Ni-*F*). $^{31}P\{^1H\}$ NMR (C_6D_6, 121.5 MHz, 298 K): major product (**7**) δ 13.6 (d, J_{PF} = 45.6 Hz). ^{19}F NMR (C_6D_6, 282.4 MHz, 298 K): minor product (**8**) δ −91.0 (m, 1F, *6-F*), −110.1 (m, 1F, *2-F*), −142.1 (m, 1F, *4-F*), −168.4 (m, 1F, *3-F*), and −387.6 (tm, 1F, Ni-*F*). $^{31}P\{^1H\}$ NMR (C_6D_6, 121.5 MHz, 298 K): minor product (**8**) δ 13.2 (d, J_{PF} = 47.4 Hz). Trace amounts of the previously reported product of C_6F_6 activation (2%), $(PEt_3)_2NiF(C_6F_5)$ (**9**), were also observed at δ −115.5, −161.2, and −163.9, along with some 1,2,4,5-tetrafluorobenzene at δ −139.5.

X-ray Crystallography. The X-ray structures were obtained at low temperature, with the crystals covered in Paratone and placed rapidly into the cold N_2 stream of the Kryo-Flex low-temperature device. The data were collected using the SMART[35] software on a Bruker APEX CCD diffractometer using a graphite monochromator with Mo Kα radiation (λ = 0.71073 Å). A hemisphere of data was collected using a counting time of 10−30 s per frame. Details of crystal data, data collection, and structure refinement are listed in Table 1. Data reductions were performed using the SAINT[36] software, and the data were corrected for absorption using SADABS.[37] The structures were solved by direct methods using SIR97[38] and refined by full-matrix least-squares on F^2 with anisotropic displacement parameters for the non-H atoms using SHELXL-97[39] and the WinGX[40] software package, and thermal ellipsoid plots were produced using ORTEP32.[41]

Calculations. Ab initio DFT calculations were performed using the hybrid functional B3LYP[42] method with the Gaussian 03 package.[43] The basis functions used were the TZVP set, provided in the Gaussian 03 program. Calculated ^{19}F NMR shielding tensors were predicted using the gauge-independent atomic orbital method that is the default of the Gaussian 03 program. The isotropic shielding values were converted to chemical shifts using a linear fit[44] to the experimental chemical shifts, given in parentheses, for a set of molecules, $CFCl_3$ (δ 0.0), hexafluorobenzene (δ −164.9), pentafluorobenzene (δ −162.3, −154.0, −139.0), SiF_4 (δ −163.3), CF_4 (δ −62.3), CFH_3 (δ −271.9), and fluorobenzene (δ −113.5). A plot of the calculated isotropic shielding values versus experimental shift was fit by a linear model with a slope of −1.11 and an intercept of −158.7. Further details are available in the Supporting Information.

For these molecules a variety of conformers are possible due to rotation around the Ni−P bonds, which complicates finding true energy minima. The different potential conformers of $\mathbf{5}^{H}$ were tested in C_2 symmetry, with all four permutations of initial P−Ni−P−H dihedral angles of 0° and 180° that define the PH_3 substituent starting conformations used as starting geometries. All the optimizations resulted in the same conformer with P−Ni−P−H closest to the 0° starting conformer. A similar test of four starting conformers of $\mathbf{5}^{Me}$ with varied P−Ni−P−C dihedral angles of C_2 symmetry resulted in two local minima, with the lowest energy conformer with four P−Ni−P−C dihedral angles closest to the 0° dihedral angle starting conformer and the alternate conformer only 0.5 kcal·mol^{-1} higher in energy. For **5**, crystallographic evidence revealed more than one conformer in the two molecules in the asymmetric unit, which suggests that the energy difference between these conformers is negligible. Thus, only the conformer with the 0° P−Ni−P−C dihedral angles as a starting point was optimized. The conformation of

(35) *SMART, Molecular analysis research tool*; Bruker AXS Inc: Madison, WI, 2001, .

(36) *SAINTPlus, Data reduction and correction program*; Bruker AXS Inc.: Madison, WI, 2001, .

(37) *SADABS, An empirical absorption correction program*; Bruker AXS Inc.: Madison, WI, 2001, .

(38) Altomare, A.; Burla, M. C.; Camalli, M.; Cascarano, G. L.; Giacovazzo, C.; Guagliardi, A.; Moliterni, A. G. G.; Polidori, G.; Spagna, R. *J. Appl. Crystallogr.* **1999**, *32*, 115–119.

(39) Sheldrick, G. M. *SHELXL-97*; Universitat Gottingen: Gottingen, 1997, .

(40) Farrugia, L. J. *J. Appl. Crystallogr.* **1999**, *32*, 837–838.

(41) Farrugia, L. J. *J. Appl. Crystallogr.* **1997**, *30*, 565.

(42) Becke, A. D. *J. Chem. Phys.* **1993**, *98*, 5648–5652.

(43) Frisch, M. J.; Trucks, G. W.; Schlegel, H. B.; Scuseria, G. E.; Robb, M. A.; Cheeseman, J. R.; Montgomery, J. A., Jr.; Vreven, T.; Kudin, K. N.; Burant, J. C.; Millam, J. M.; Iyengar, S. S.; Tomasi, J.; Barone, V.; Mennucci, B.; Cossi, M.; Scalmani, G.; Rega, N.; Petersson, G. A.; Nakatsuji, H.; Hada, M.; Ehara, M.; Toyota, K.; Fukuda, R.; Hasegawa, J.; Ishida, M.; Nakajima, T.; Honda, Y.; Kitao, O.; Nakai, H.; Klene, M.; Li, X.; Knox, J. E.; Hratchian, H. P.; Cross, J. B.; Bakken, V.; Adamo, C.; Jaramillo, J.; Gomperts, R.; Stratmann, R. E.; Yazyev, O.; Austin, A. J.; Cammi, R.; Pomelli, C.; Ochterski, J. W.; Ayala, P. Y.; Morokuma, K.; Voth, G. A.; Salvador, P.; Dannenberg, J. J.; Zakrzewski, V. G.; Dapprich, S.; Daniels, A. D.; Strain, M. C.; Farkas, O.; Malick, D. K.; Rabuck, A. D.; Raghavachari, K.; Foresman, J. B.; Ortiz, J. V.; Cui, Q.; Baboul, A. G.; Clifford, S.; Cioslowski, J.; Stefanov, B. B.; Liu, G.; Liashenko, A.; Piskorz, P.; Komaromi, I.; Martin, R. L.; Fox, D. J.; Keith, T.; Al-Laham, M. A.; Peng, C. Y.; Nanayakkara, A.; Challacombe, M.; Gill, P. M. W.; Johnson, B.; Chen, W.; Wong, M. W.; Gonzalez, C.; Pople, J. A. *Gaussian 03*, revision C.01; Gaussian, Inc.: Wallingford, CT, 2004, .

(44) (a) Fukaya, H.; Ono, T. *J. Comput. Chem.* **2003**, *25*, 51–60. (b) Sanders, L. K.; Oldfield, E. *J. Phys. Chem. A* **2001**, *105*, 8098–8104. (c) Chan, J. C. C.; Eckert, H. *THEOCHEM* **2001**, *535*, 1–8.

the P−C−C bond angles of the ethyl substituents was taken from the crystal structure as a starting point in this DFT optimization. The optimized geometry has C_2 symmetry.

Three different starting conformations of the mononuclear adduct $\mathbf{6}^{H}$ were optimized to local minima, with two having C_s symmetry and identical starting P−Ni−P−H dihedral angles of 0° and 180°, and one conformer having C_1 symmetry and different starting P−Ni−P−H dihedral angles of 0° and 180°. These provided three local minima, with the lowest energy conformer corresponding to the C_s symmetric species with optimized P−Ni−P−H angles that started at 0°. The other conformers were a maximum of 0.4 kcal·mol^{-1} higher in energy. Three different starting conformations for $\mathbf{6}^{Me}$ were also investigated. The lowest energy conformer was a C_s symmetric species optimized from P−Ni−P−C angles starting at 0°. The other conformers were a maximum of 0.2 kcal·mol^{-1} higher in energy. The C_s symmetric structure for the mononuclear $Ni(PEt_3)_2$ adduct, **6**, was found to have an imaginary frequency. A minimum energy C_1 symmetric structure was located.

The dinuclear adducts of C_6F_5H, $\mathbf{1a}-\mathbf{c}^{H}$, $\mathbf{1a}-\mathbf{c}^{Me}$, and **1a**, as well as the mononuclear adducts $\mathbf{2a}-\mathbf{c}^{H}$, $\mathbf{2a}-\mathbf{c}^{Me}$, and **3a**,**c** were optimized starting from the geometries obtained with the C_6F_6 analogues; all these species have local minima with C_1 symmetry. The hydrides $\mathbf{3}^{H}$, $\mathbf{3}^{Me}$, and **3** were all found to have local minima with C_2 symmetry.

Acknowledgment is made to the National Sciences and Engineering Council (NSERC) of Canada and the Shared Hierarchical Academic Research Computing Network (SHARCNET) for their support.

Supporting Information Available: Full details of ref 41; crystallographic information in CIF format for **1**, **2**, and **5**; select experimental NMR spectra, optimized coordinates, and energies for DFT calculations. This material is available free of charge via the Internet at http://pubs.acs.org.